Journal of Volcanology and Geothermal Research 401 (2020) 106944

Contents lists available at ScienceDirect

Journal of Volcanology and Geothermal Research

journal homepage: www.elsevier.com/locate/jvolgeores

Standing waves in high speed lava channels: A tool for constraining lava dynamics and eruptive parameters

Y. Le Moigne [a,b,*], J.M. Zurek [a], G. Williams-Jones [a], E. Lev [c], A. Calahorrano-Di Patre [a], J. Anzieta [a]

[a] Centre for Natural Hazards Research, Department of Earth Sciences, Simon Fraser University, Burnaby, BC, Canada
[b] Laboratoire Magmas et Volcans, Université Clermont Auvergne, 63178 Aubière, France
[c] Lamont-Doherty Earth Observatory, Columbia University, Palisades, NY, USA

ARTICLE INFO

Article history:
Received 29 January 2020
Received in revised form 16 May 2020
Accepted 26 May 2020
Available online 30 May 2020

Keywords:
Standing waves
Hydraulic jumps
Supercritical flow
Lava viscosity
Lava flow
Basalt
Real time monitoring

ABSTRACT

Estimates of the rheological properties of lava flows are essential for understanding their emplacement and for hazard assessment. Despite being a well-known phenomenon in water hydraulics, the formation and presence of standing waves in lava channels is poorly understood. Standing waves, generally located near the vent area, have been frequently described at high speed channelized lava flows. They are interpreted as hydraulic jumps indicating a flow under supercritical conditions. Identifying standing waves therefore offers an opportunity to apply open channel hydraulic theory for supercritical flows in order to determine important eruption parameters such as discharge rate and apparent viscosity. We use the length and amplitude of standing waves to reconstruct flow dynamics from both observational data and video analysis. The geometry of these standing waves allows us to extract the physical properties of the channelized lava (velocity, discharge rate, apparent viscosity), to estimate the channel depth and constrain the flow regime. With the rapid advances in technology, scientists can deploy equipment to enable low-cost real time monitoring of these phenomena and constrain eruption discharge rate and apparent viscosity, key parameters for volcanic hazard assessment and mitigation.

1. Introduction

Basaltic lava flows are the most abundant product of effusive volcanic eruptions on Earth and other planets (Kilburn, 2000). Their emplacement has been extensively studied over the past decades from direct observations of active or historical lava flows, lab experiments and mathematical modelling (e.g., Walker, 1973; Hulme, 1974; Lipman and Banks, 1987; Pinkerton and Wilson, 1994; Crisp et al., 1994; Harris and Rowland, 2001; Guilbaud et al., 2005; Lev et al., 2012; Cashman et al., 2013; Chevrel et al., 2013, 2019; Cashman and Mangan, 2014; Cordonnier et al., 2016). Lava flow emplacement is governed by the relationship between lava rheology (as a function of composition, temperature and texture), the rate at which the lava is extruded, and environmental conditions such as topography and cooling (e.g., Shaw et al., 1968; Crisp et al., 1994; Pinkerton and Wilson, 1994; Griffiths, 2000; Harris and Rowland, 2001; Chevrel et al., 2013; Kolzenburg et al., 2017). When channelized, these flows can travel long distances, sometimes at high velocities, which increases their potential threat to local communities (Rowland et al., 2005; Behncke et al., 2005; Kauahikaua, 2007; Crisci et al., 2008; Favalli et al., 2009; Neal et al., 2019). Observations and estimates of the rheological properties of basaltic lava have shown that active lava flows can reach velocities up to the order of 10 m/s and with viscosities lower than 10^3 Pa·s (Baloga et al., 1995; Lipman and Banks, 1987; Griffiths, 2000; Geist et al., 2008; Lesher and Spera, 2015; Chevrel et al., 2018). Griffiths (2000) shows that under such conditions a lava flow can be in a supercritical state, potentially exhibiting similar hydraulic jumps and standing waves observed and described in classic open channel studies.

While numerous studies have described high speed channelized lava flows with standing waves (e.g., Finch and MacDonald, 1953; Richter et al., 1970; Wolfe, 1988; Heslop et al., 1989; Woodcock, 2003; Woodcock and Harris, 2006; Geist et al., 2008; Cashman and Mangan, 2014; Cashman et al., 2018), only a few to our knowledge (Cashman et al., 2018) have used these observations to determine flow parameters such as discharge rate and lava viscosity. In this study we show that these lava flows can meet all conditions for supercritical flow and the derived hydraulic jumps. This observation creates an opportunity to apply open channel fluid hydraulics for rapidly varied flows and supercritical flows in order to determine important eruption parameters including channel depth, flow velocity, discharge rate and apparent viscosity. This approach can also provide critical forecasting information such as lava flow length, a key parameter in hazard mitigation and civil protection.

* Corresponding author at: Centre for Natural Hazards Research, Department of Earth Sciences, Simon Fraser University, Burnaby, BC, Canada.
E-mail address: ylemoign@sfu.ca (Y. Le Moigne).

https://doi.org/10.1016/j.jvolgeores.2020.106944
0377-0273/

2. Open channel flow: overview and definitions

The definitions below assume a channelized Newtonian fluid. We will show in Section 3 that under specific conditions (i.e., viscosity $<10^3$ Pa·s and velocity of several m/s), a lava flow can be approximated as a Newtonian fluid, so that the following equations are relevant if such lava flows are channelized. We define open channel flow as a liquid flowing in a conduit with a free surface and driven by gravity alone. The free-surface is the interface between the liquid and the ambient atmosphere and is subject to a pressure that is equal to the local atmospheric pressure, usually negligible. Fluvial systems, such as rivers or creeks as well as human-made infrastructure such as irrigation channels, sewers, spillway dams show open channel flows. A moving fluid in an open channel can be described according to its turbulence and critical state. All parameters used for the following equations are given in Table 1.

2.1. Turbulence state and Reynolds number

The turbulence state of the flow is given by the Reynolds number, *Re*, which is the ratio of the inertial force to the viscous force:

$$Re = \frac{\rho v D}{\eta} \tag{1}$$

where, ρ and η are the density (kg/m^3) and the viscosity (Pa·s) of the fluid in motion, respectively. v is the fluid velocity (in m/s) and in an open channel flow, D is the hydraulic diameter (m) of the channel under consideration. The hydraulic diameter is defined as four times the channel cross sectional area, $A = H \times W$ (m^2; with H the channel depth and W the channel width), divided by the wetted perimeter, P_W (m):

$$D = \frac{4A}{P_W} \tag{2}$$

The wetted perimeter, P_W, corresponds to the channel perimeter that is in contact with the fluid. In open channel hydraulics, P_W is related to the channel bottom and wall lengths. For a rectangular channel, P is two times the channel depth plus the channel width:

$$P_W = 2H + W \tag{3}$$

A fluid is called laminar when the particles appear to move along straight paths, generally occurring when $Re < 2000$. In contrast, fluid is considered turbulent when the particles move along irregular paths, indicating $Re > 2000$. The transition from laminar to turbulent occurs between $500 < Re < 2000$, sometimes referred to as transitional flow (e.g., Chow, 1959).

2.2. Critical state, Froude number and hydraulic jumps

The conditions for critical, subcritical and supercritical flow for an incompressible fluid are resolved from the laws of conservation (continuity and momentum conservation; e.g., Chow, 1959; Chanson, 2004). Assuming the conditions represented in Fig. 1 and that the pressure is hydrostatic (i.e., $P = \rho g H$), integration of the Bernoulli equation implies that the total head at the channel section is a constant:

$$z + H\cos\alpha + \gamma\frac{v^2}{2g} = Be = constant \tag{4}$$

where α is the channel slope (°) and z the vertical distance above a reference plane (m), $v^2/2g$ is the velocity head and H the flow depth with respect to the channel slope. Due to shear stress at the bottom and side walls, the flow velocity distribution in a channel is not uniform, especially in the vertical and transverse direction (i.e., z and y directions). Therefore, the velocity in a channel cross section varies from point to point, with maximum velocities usually located near the top and centre of the channel and minimum velocities along the channel walls and bottom (e.g., Fig. 1.9 and 1.10 in Chow, 1959). Based on the work of Chow (1959), a dimensionless kinetic correction factor, γ, is introduced in Eq. (4) to correct this difference of velocities in the channel cross-section. This factor is sometimes called the Coriolis coefficient (Chow, 1959; Field et al., 1998; Yen, 1973; Chaudhry, 2008). In natural system γ is always >1 and can be as great as 2 in complex and compound natural channel cross sections (Chow, 1959; Henderson, 1966; Chaudhry, 2008). However, considering simple channel cross-sections such as

Table 1
Notation and symbols used. Subscripts 1 and 2 refer to upstream and downstream conditions of the hydraulic jump.

Symbol	Unit	Definition
A	m^2	Channel cross-section
A_j	m	Amplitude of a hydraulic jump
B	–	Bingham number
Be	m	Integral form of the Bernoulli equation
D	m	Hydraulic diameter
E_S	m	Specific energy per unit mass of the fluid
Fr	–	Froude number
f	–	Fanning friction factor
G	–	Ratio of buoyancy to viscous stresses
g	m/s^2	Gravitational acceleration
H	m	Lava flow depth
H_C	m	Critical depth
K	–	Coefficient depending on channel shape and roughness
L_j	m	Length of hydraulic jump
P	Pa	Pressure
P_W	m	Wetted perimeter
Q	m^3/s	Lava flow discharge rate
Re	–	Reynolds number
r	m	Average height of channel wall irregularities
v	m/s	Lava flow velocity
W	m	Channel width
z	m	Elevation above reference datum
α	°	Channel slope angle
β	°	Oblique hydraulic wave front angle with respect to original wall direction
γ	–	Kinetic energy correction factor for non-uniform velocity gradient in channel cross-section; or Coriolis coefficient
	s^{-1}	Strain rate
η	Pa·s	Lava flow viscosity
θ	°	Bending angle of one channel wall with respect to original wall direction
ρ	kg/m^3	Lava flow density
σ_0	Pa	Yield stress
τ_s	N/m^2	Shear stress
Ω	m^2/s^2	$=4v_1^2(v_1^2 - 3\omega A_j) + (\omega A_j)^2$
ω	m/s^2	$=g\cos\alpha$

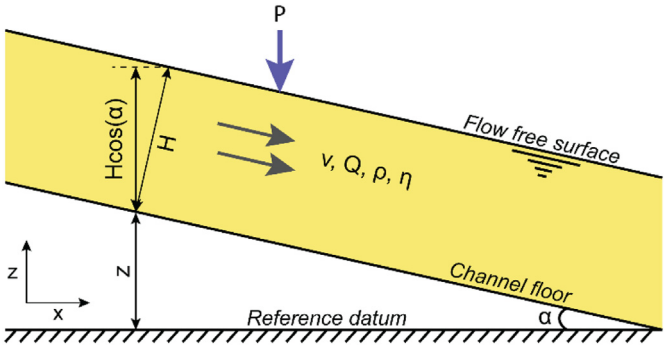

Fig. 1. Open channel flow on a sloped surface. The free surface is subject to the atmospheric pressure, *P*. This diagram is shown parallel to a streamline at the centre of the channel (i.e., parallel to the x-axis and perpendicular to the y-axis). Definitions of the symbols are given in Table 1.

square, U-shape or rectangular sections, γ is slightly above unity and can be neglected (i.e., $\gamma = 1$; Chow, 1959).

By analyzing the specific energy, we can determine under which conditions the flow is critical, sub- or supercritical. If the contribution from the potential energy is removed from Eq. (4) ($Be - z$), the specific energy, E_S is found, which is analogous to the energy per unit mass of the flow measured in relation to the channel floor. In a channel cross section, E_S is thus (Chow, 1959; French, 1986; Chaudhry, 2008):

$$E_S = H\cos\alpha + \gamma\frac{v^2}{2g} \tag{5}$$

Fig. 2 shows a plot of the flow energy, E_S, versus depth of flow, H, for a given sloped rectangular channel and a variety of discharge rates, Q (m^3/s). For illustrative purposes, we choose the following parameters: channel width, $W = 15$ m; channel slope, $\alpha = 10°$; discharge rate, $Q = 10$, 50, 100, 200 and 1000 m^3/s. At large values of depth, E_s is high because the flow depth, H is large. For very small values of H, E_s is high because the velocity is high resulting in a high velocity head ($v^2/2g$). Critical flow conditions occur when E_S is minimum; these critical points are shown by the white diamonds on Fig. 2 for each of the analyzed discharge rates. In this geometry, these conditions are reached when the velocity head is equal to half the contribution of the pressure head (Chow, 1959):

$$\gamma\frac{v^2}{2g} = \frac{H\cos\alpha}{2} \tag{6}$$

Rearranging Eq. (6), the critical state can be written as the ratio of the contribution of inertial forces of the fluid to the gravitational forces, and is represented by the dimensionless Froude number, Fr (Chow, 1959; Hager, 1985; French, 1986; Chaudhry, 2008). For an idealized frictionless sloped rectangular channel:

$$Fr = \frac{v}{\sqrt{gH\cos\alpha/\gamma}} \tag{7}$$

A flow is critical when $Fr = 1$, subcritical when $Fr < 1$ and supercritical when $Fr > 1$. As previously mentioned, γ can be neglected for rectangular channels; therefore, from the above equation, the critical flow depth H_C is:

$$H_C = \frac{v^2}{g\cos\alpha} \tag{8}$$

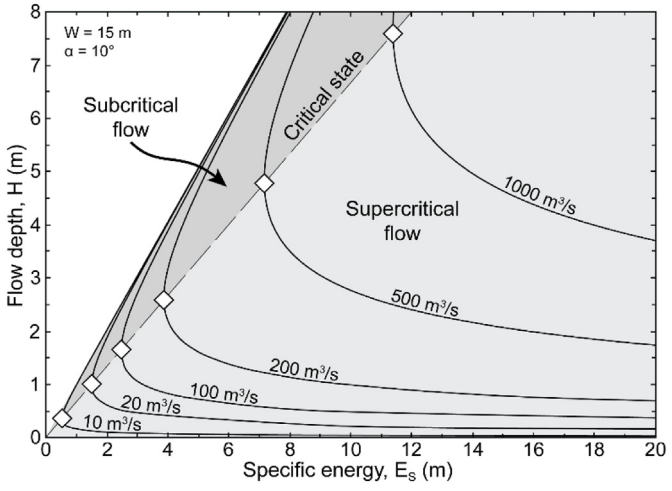

Fig. 2. Specific energy curves in a sloped rectangular open channel with W = 15 m, α = 10° and Q = 10, 20, 100, 200, 500 and 1000 m^3/s. The specific energy is the sum of the velocity head and pressure head with respect to the channel slope. The critical depth for each discharge rate scenario is shown by a white diamond. This is the depth at which the flow is in a critical state, i.e., $Fr = 1$ and possesses the lowest amount of energy. Above this point, the flow is in a subcritical state ($Fr < 1$, i.e., low velocities, deep flows). Inversely, below the critical point, flow is in a supercritical state ($Fr > 1$, shallow depths, high velocities).

A hydraulic jump is the abrupt transition of a flow from a supercritical to subcritical state. Whenever a flow in supercritical state occurs in a channel that cannot sustain it, a hydraulic jump will develop to convert the flow to a subcritical state. When the Froude number is slightly larger than one, the hydraulic jump is characterized by a smooth rise of the free-surface perpendicular to the flow direction, often followed by a train of stationary free-surface undulations called standing waves (Fig. 3): this is referred to as the undular hydraulic jump (Chow, 1959; Hager and Hutter, 1984; Montes and Chanson, 1998; Ohtsu et al., 2003; Chanson, 2009). Undular hydraulic jumps can be observed in horizontal channels and at transitions between steeper and milder channel slopes (Hager and Hutter, 1984; Ohtsu et al., 2003). Undular hydraulic jumps are naturally observed in channels with Froude number up to 3–4 depending on the channel slope, channel walls' roughness and upstream flow conditions (Bradley and Peterka, 1957; Hager and Hutter, 1984; Chanson, 2009). For a supercritical fluid moving in a bent channel such as in Fig. 4, a particular hydraulic jump called an oblique jump occurs (Hager et al., 1994; Ippen and Harleman, 1956; Chaudhry, 2008). For a more detailed description and classification of hydraulic jumps, we refer the reader to Appendix A.

The phenomenon of hydraulic jump and the Froude number are widely used in water hydraulics and fluvial studies (e.g., Chow, 1959; Kieffer, 1985, 1987; Tinkler, 1997a, 1997b; Comiti and Lenzi, 2006; Magirl et al., 2009). However, the description of supercritical flows in Earth science disciplines is infrequent. In sedimentology, hydraulic jumps and the Froude number are used to explain the formation of particular bedforms such as *antidunes* or '*chutes-and-pools*' (e.g., Fralick, 1999; Alexander et al., 2001; Lenzi, 2001; Duller et al., 2008; Macdonald et al., 2013; Cartigny et al., 2014). In volcanology, the deposition of breccia and lithics at slope breaks from pyroclastic density currents are often interpreted as the result of hydraulic jumps (e.g., Freundt and Schmincke, 1985; Roobol et al., 1987; Cole et al., 1998; Macías et al., 1998).

3. Conditions for supercritical lava flows

Lava flows are typically considered as a three-phase fluid (melt with suspended crystals and bubbles) of viscosity η and yield stress σ_0 (cf. Pinkerton and Stevenson, 1992; Harris and Allen, 2008; Chevrel et al., 2013; Mader et al., 2013; Truby et al., 2015). For the purpose of argument, we assume that a lava flow with a constant viscosity behaves as a Bingham fluid (Hulme, 1974; Shaw et al., 1968; Dragoni et al., 1986; Pinkerton and Norton, 1995; Griffiths, 2000; Morrison et al., 2020) and we show that under certain conditions that leads to a Newtonian regime.

We consider a basaltic lava of depth H, flowing in a sloped rectangular channel of width W and slope α. We set the x-axis as the centre line of the channel and parallel to the reference datum, the y-axis is perpendicular to the flow direction and the z-axis is the normal to the flow free surface (Fig. 1). In these conditions, the horizontal momentum of a lava flow on the sloping plane is (Balmforth et al., 2000; Griffiths, 2000):

$$\rho\frac{Dv_i}{Dt} = -\frac{\partial P}{\partial x_i} + \left(\frac{\partial}{\partial y} + \frac{\partial}{\partial z}\right)\left(2\left(\eta + \frac{\sigma_0}{\varepsilon}\right)\varepsilon_{ij}\right) + \rho g\sin\alpha \tag{9}$$

where t is the time, v_i is the velocity along the maximum flow direction, P is the pressure, ρ is the density, g is gravity and is the strain rate that represents the local deformation of the velocity field after an infinitesimal displacement of the fluid in the x, y and z directions. With appropriate rescaling, the Reynolds number multiplies , and the term turns into

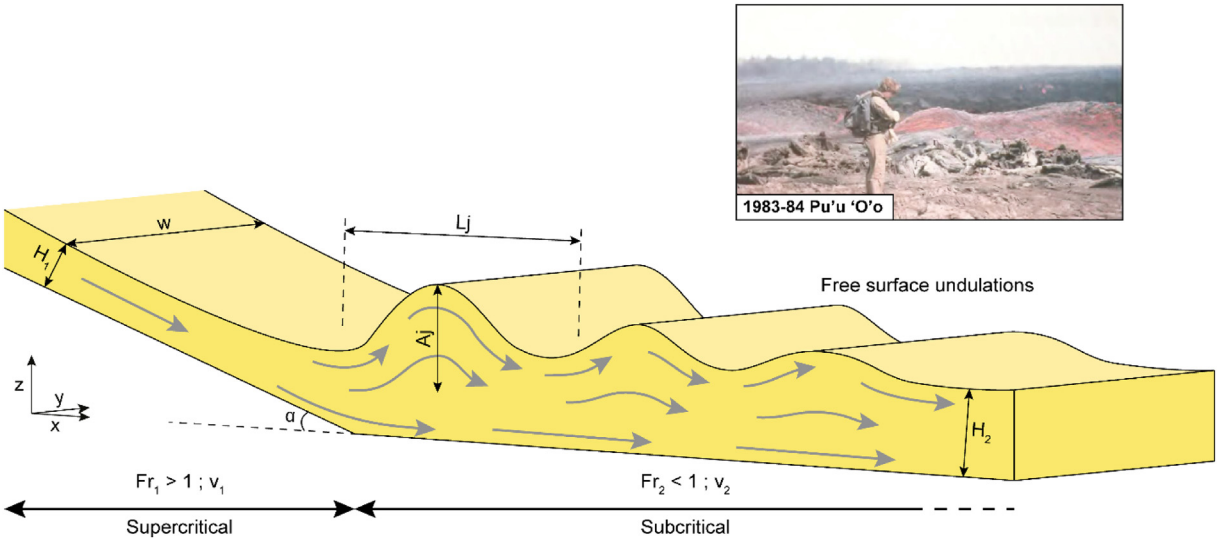

Fig. 3. Schematic diagram of a lava flow in a rectangular channel exhibiting a non-breaking undular hydraulic jump at a break in slope. This diagram represents the conditions in the centre of the channel ($w < W$). Not shown here, are the lateral shock waves along the channel side walls. An undular hydraulic jump is produced when a supercritical flow transforms into a subcritical flow. This phenomenon produces a standing wave of length L_j and height A_j usually followed downstream by several free surface undulations. Inset shows standing waves in a channelized lava flow during the 1983–84 eruption of Pu'u 'O'o (from Wolfe, 1988).

with B the dimensionless Bingham number defined as . For a Newtonian flow approximation, $\sigma_0 \to 0$, therefore $B \to 0$ (Dragoni et al., 1986; Griffiths, 2000).

Near the vent, the temperature of freshly erupted basaltic lavas are >1100 °C and when channelized, these lava flows can reach velocities of ~10 m/s with viscosities on the order of 10^1–10^3 Pa·s (Lipman and Banks, 1987). With channel depth of 1–10 m and assuming lava density of 2600 kg/m^3 (unvesiculated basalt; Lesher and Spera, 2015) to 500 kg/m^3 (~80% vesicles; Cashman et al., 1994), these flows have Reynolds numbers of ~10^2–10^3 and strain rates of ~10^0–10^{-1} s^{-1} (Dragoni et al., 1986; Griffiths, 2000; Lev et al., 2012; Kolzenburg et al., 2017; Chevrel et al., 2019). Under such conditions, at high velocities the lava has not undergone significant cooling (e.g., absence of a cool surface crust), is isothermal, the yield strength is negligible with respect to viscous forces (i.e., $\sigma_0 < 10^3$ Pa) and thus closely behaves as a Newtonian fluid (Dragoni et al., 1986; Pinkerton and Stevenson, 1992; Griffiths, 2000; Tallarico and Dragoni, 1999; Chevrel et al., 2019; Harris et al., 2020). Therefore, given these conditions, B may be on the order of 10^{-1}–10^{-3}. Hence, with $Re \sim 10^2$–10^3, $Re \gg (1+B)$ and Eq. (9) becomes (Balmforth et al., 2000; Griffiths, 2000):

$$\frac{Re}{G} = \frac{v^2}{gH} = Fr^2 \cos\alpha \tag{10}$$

where, G is the ratio of buoyancy to viscous stresses (Griffiths, 2000) and Fr is the Froude number as defined in Eq. (7). This shows that for channelized lava flows at velocities of ~10 m/s, the Froude number becomes a relevant parameter that may potentially be larger than unity, indicating a lava flow under supercritical conditions (Fig. 5; Griffiths, 2000). If such conditions are achieved, the channelized lava flows can exhibit hydraulic jumps as standing waves.

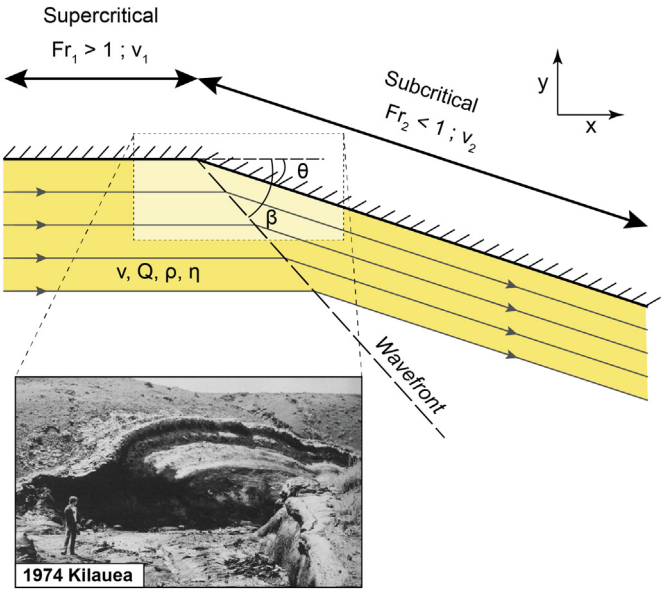

Fig. 4. Schematic diagram of a channelized lava flow exhibiting an oblique hydraulic jump in plan view. This diagram represents the conditions on the left side of the channel. The right side of the lava channel is not shown. The wavefront of the oblique hydraulic jump originates from the point of bending of the channel and makes an angle β with respect to the original channel wall direction. β should satisfy $\theta < \beta < 90°$, with θ the channel bend angle (modified from Ippen and Harleman, 1956). The inset shows preserved super-elevated levees at a channel bend after the 1974 eruption of Kīlauea (from Heslop et al., 1989).

4. Observed standing waves in lava channels and interpretations

4.1. Observations of standing waves in lava channels

Several studies have described standing waves occurring in basaltic lava flows (Fig. 6). We have tabulated in Appendix B all reported occurrences of standing waves, hydraulic jumps or supercritical flows in channelized lava flows. The term '*hydraulic jump*' was first used to describe a standing wave in a high speed lava channel during the June 1950 southwestern rift zone eruption of Mauna Loa volcano, Hawai'i by Finch and MacDonald, 1953. In 1950, Mauna Loa volcano erupted 376 × 10^6 m^3 in <23 days, with lava channels reaching the sea. The volumetric eruption rate was amongst the largest ever recorded on Mauna Loa (Finch and MacDonald, 1953; Rowland and Walker, 1990). On June 7, an incandescent lava channel flowed over an 8 m high cascade at an estimated velocity of 13 m/s. Immediately downstream of the cascade, "*the rush of the liquid lava*" formed a standing wave referred to as a

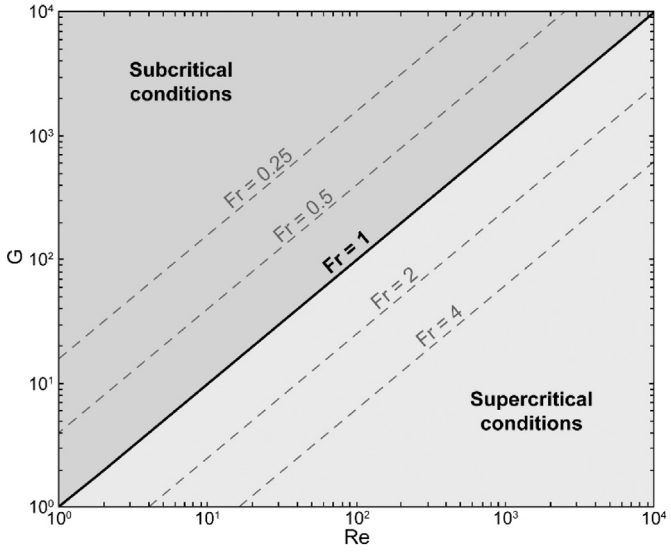

Fig. 5. Reynolds number, *Re*, plotted against the ratio of buoyancy to viscous stresses, *G*, for a rectangular channel. The bold line $Fr = 1$ represents lava flow under critical conditions. Below this line, the lava is in supercritical conditions, $Fr > 1$ whereas above the lava is in subcritical conditions, $Fr < 1$.

hydraulic jump 1.2–1.4 m high (Finch and MacDonald, 1953). A surge of lava observed at the vent feeding the lava channel was noted just before the wave increased to ~3.6 m in height.

During the 1983–84 eruption of Pu'u 'O'o, Kīlauea, Hawai'i, standing waves were described as a common phenomenon in high speed lava channels (8 to 15 m/s; Fig. 6a) in close proximity to the vents (Wolfe, 1988). Notably, several standing waves in lava channels were observed during Episodes 4, 10, 11, 17 and 18 of the eruption (Fig. 6a; Takahashi and Griggs, 1987; Wolfe, 1988). During Episode 4 (June 13–17, 1983), the Pu'u 'O'o crater was partially filled by a lava pond. The lava escaped the crater through a 3–5 m wide spillway and fed the main flow of this eruptive episode (Wolfe, 1988). At the bottom of this spillway, a "*spectacular standing wave*" was frequently observed throughout the entire eruptive episode (Wolfe, 1988). In the spillway, the estimated velocity was ~15 m/s and had an estimated discharge rate of ~160 m^3/s assuming a lava depth of 3 m (Wolfe, 1988). At about 200 m from the Pu'u 'O'o vent, near the end of Episode 10 (October 5–7, 1983), a series of standing waves several metres high and 10–15 m long, in a 10–15 m wide lava channel, were observed after a surge in lava discharge rate from the vent (Wolfe, 1988). During Episode 11 (November 5–7, 1983), a series of 5 standing waves were observed over a length of 150–200 m in a lava channel ("*a vigorous pahoehoe river*"; Fig. 6a) located ~100 m from the vent (Wolfe, 1988). The channel was ~15 m wide, with estimated surface flow velocities of 8–10 m/s. These standing waves were located at a break in slope (from 10° to 2°) and each wave was 20–40 m long and 1–3 m high; the flow slowed after the standing wave zone (Wolfe, 1988). Discharge rates in this channel were calculated at between 278 and 556 m^3/s (Wolfe, 1988). On the first day of Episode 17 (March 30–31, 1984), a "*voluminous torrent of lava*" exited the Pu'u 'O'o crater through a >10 m wide spillway that fed a lava channel. The underlying slope of the channel at the base of the Pu'u 'O'o cone was gentle. Standing waves several metres high and >15 m long were located at this break in slope (Wolfe, 1988). Finally, a few standing waves ~2 m high and ~ 10 m long were observed in lava channels at the bottom of Pu'u 'O'o cone during Episode 18 (April 18–21, 1984; Wolfe, 1988).

Between March 25 and April 14, 1984, Mauna Loa volcano erupted and produced a ~25.6 km long and ~0.224 km^3 basaltic lava flow in the northeast rift zone (Lipman and Banks, 1987). This large flow developed a channel system that was active and stable for several days from March 30 to April 7 (Lipman and Banks, 1987). Standing waves were observed between April 1 and April 6 about 150 m from the vent (Fig. 6b). A video recording of these standing waves was made by J. D. Griggs on April 2 (Griggs, 1984; https://www.usgs.gov/media/videos/mauna-loa-lava-flow-april-2-1984), and shown in the documentary "*Rivers of Fire*" (Malzman, 1985) as well as in the movie "*Into the Inferno*" (Herzog, 2016). According to these recordings, the standing waves were located in a secondary channel separated from the main channel by a kipuka.

Sierra Negra volcano, Galápagos, Ecuador, erupted 150×10^6 m^3 of lava over 9 days in October 2005 (Geist et al., 2008). During this eruption, the lava flowed down the summit caldera benches (slopes of

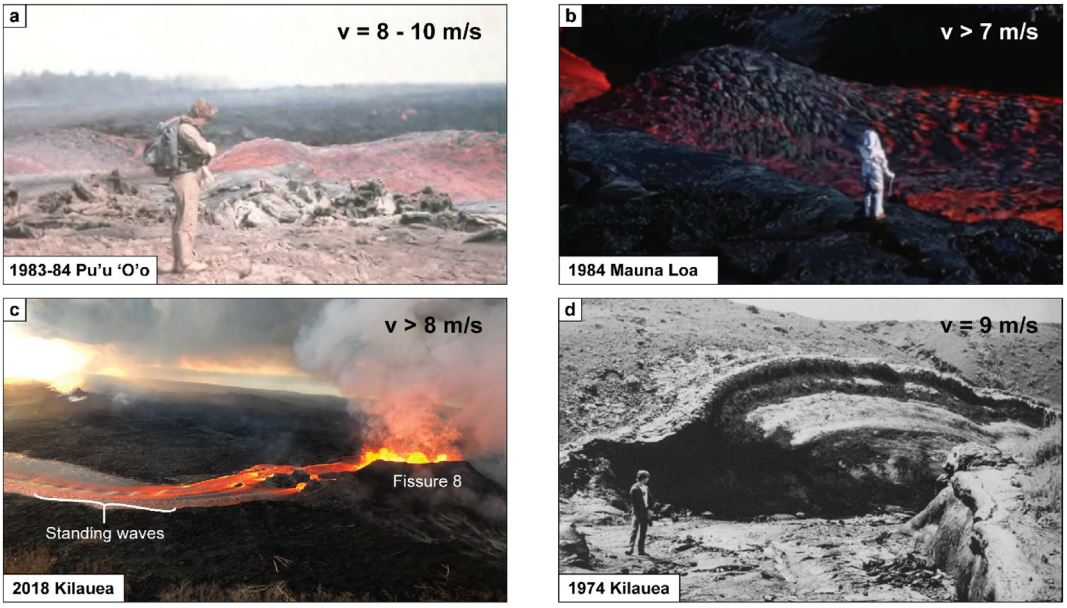

Fig. 6. Standing waves in high speed lava channels. (a) A series of stationary undulating wave during the eruption of Pu'u 'O'o in 1983–84 (Wolfe, 1988). (b) Non-breaking undular hydraulic jump in a lava channel during the 1984 eruption of Mauna Loa (screenshot from the movie "*Into the Inferno*" by Herzog (2016)). (c) Standing waves during the eruption of Fissure 8, Kīlauea, in 2018 (photo taken on Wednesday, June 13, 2018; USGS Hawaiian Volcano Observatory). (d) Preserved super-elevated levees at a channel bend by an oblique hydraulic jump after the eruption of Kīlauea in 1974 (Heslop et al., 1989).

~15°) in channels at an estimated velocity of ~15 m/s. Standing waves of lava >5 m high were observed at the bottom of the caldera benches (Geist et al., 2008).

Furthermore, standing waves in high speed lava channels were also observed during the first phase of the 1959 summit eruption of Kīlauea (Richter et al., 1970), during the Lower East Rift Zone eruption of Kīlauea in 2018 (Fig. 6c; Cashman et al., 2018; Patrick et al., 2019). During the 2014–2015 eruption of Holuhraun (Iceland), near the eruptive vent, standing waves were also observed both at breaks in slope and at channel bends (S. Kolzenburg, personal communication).

During 3 days in July 1974, Kīlauea volcano, erupted and a fissure system was active on the southeastern Kīlauea caldera rim (Heslop et al., 1989). This fissure fed a lava flow into a 230 m long confined gully valley, called the '*gully flow*' (Heslop et al., 1989). At about 100 m from the fissure system, the gully makes a 45° turn and exhibits spectacular super-elevated levees (Fig. 6d). Indeed, on the outer bend of the channel, the height of the levees is higher than the average flow depth. It was suggested that a supercritical lava flow with standing waves could have been responsible for the raised levees (Heslop et al., 1989).

According to Kauahikaua et al. (1998), standing waves are a common phenomenon in lava tubes when the lava is flowing at several m/s at breaks in slope. A long-lived standing wave was witnessed in a lava tube by Kauahikaua et al. (1998) at the foot of a small lava cascade. This standing wave was observed through a lava tube skylight for almost a year in 1996 in lava flowing at 5.6 m/s in the tube. The wave was located at an 80° sharp turn at the foot of a lava cascade (Kauahikaua et al., 1998).

4.2. Summary and interpretations

From the above descriptions of standing waves, the following conclusions can be made:

1. All the standing waves were observed in lava channels (Finch and MacDonald, 1953; Richter et al., 1970; Lipman and Banks, 1987; Takahashi and Griggs, 1987; Wolfe, 1988; Geist et al., 2008; Cashman et al., 2018). One example of a standing wave was noted in a lava tube (Kauahikaua et al., 1998). They represent free surface flow in open channels.
2. Standing waves, by definition, were stationary in space and they propagated through time. Although the geometry of the standing waves varied in time (due to changes in the lava discharge rate; Finch and MacDonald, 1953; Kauahikaua et al., 1998; Wolfe, 1988; Geist et al., 2008), they were observed for a significant amount of time (hours to months). For example, the standing wave described by Kauahikaua et al. (1998) was observed for several months at the same location. The preserved super-elevated levees described by Heslop et al. (1989) in the 1974 Kīlauea '*gully flow*' also indicate a certain duration in time of the oblique standing wave.
3. Observed standing waves always occurred in high speed lava channels. An estimated speed of ~15 m/s just upstream of standing waves was reported during Episode 4 of the 1983–84 Pu'u 'O'o eruption (Wolfe, 1988) and during the 2005 Sierra Negra summit eruption (Geist et al., 2008). The minimum reported velocity for a lava standing wave is 5.6 m/s (Kauahikaua et al., 1998).
4. The standing waves were usually located in close proximity to the vent. Standing waves were seen in vent spillways during the 1983–84 Pu'u 'O'o eruption (Episodes 4 and 17) or within a few hundred metres of the base of Pu'u 'O'o (Episodes 10, 11 and 18; Wolfe, 1988). The only exception was the long-lived standing wave located at about 4.1 km from the feeding vent (Kauahikaua et al., 1998).
5. All the observed standing waves were located at channel disruptions; at a break in slope (Finch and MacDonald, 1953; Wolfe, 1988), the bottom of a spillway or at small lava cascades (Richter et al., 1970; Kauahikaua et al., 1998; Wolfe, 1988), the base of caldera benches (Geist et al., 2008), or at channel bends (Heslop et al., 1989).

During Episode 4 of the Pu'u 'O'o eruption, a lava velocity of ~15 m/s was estimated just upstream of a standing wave in a channel of ~3 m depth. Applying the Froude number equation (Eq. (7)), the $Fr_1 \approx 2.7$. For most of the other examples, the channel depth and slope are not reported or are unknown. However, assuming reasonable flow depths ($H_1 = 1$–5 m) and channel slopes (α up to 20°), we obtain a $Fr_1 \sim 1.1$–3. This indicates lava under supercritical conditions where the standing waves were observed. We propose that these standing waves were the result of hydraulic jumps.

These lava standing waves possessed similar characteristics to the undular standing wave (Appendix A; Chow, 1959; Hager and Hutter, 1984; French, 1986; Hager, 1992; Montes and Chanson, 1998; Chaudhry, 2008; Chanson, 2009):

- In many cases, the first standing wave was followed downstream by a series of free-surface stationary undulations. They were spaced ~10–20 m over tens to a few hundred metres. When reported, the amplitudes were up to ~5 m.
- Rough calculations give $Fr_1 \leq 3$. According to Chanson (2009), undular standing waves can naturally occur for Fr_1 up to 4.

5. Estimation of lava flow dynamics from hydraulic jump characteristics

Here we provide the procedure to estimate the velocity, v (m/s), discharge rate, Q (m^3/s), the depth, H (m), and apparent viscosity, η (Pa·s) for lava flows in a supercritical state undergoing a hydraulic jump (Figs. 3, 4). For the derivations below, the subscripts *1* and *2* refer to upstream and downstream conditions of the hydraulic jump, respectively.

5.1. Assumptions

Our analysis assumes that:

1. Flow (of depth H) is in a sloped rectangular channel (width W, slope α) in order to minimise the number of starting parameters and unknowns (Lev and James, 2014);
2. For undular jumps (Appendix A), the following analysis is valid along a streamline located at the centre of the channel. For simplification, we do not take into account the effect of the lateral shockwave that develops from the channel side walls for $Fr_1 > 1.2$ (Appendix A; Montes and Chanson, 1998; Ohtsu et al., 2003).
3. The lava is modeled as a single-phase material with a Newtonian rheology – although lava flows are typically considered as three-phase fluids with complex strain-rate-dependent rheology (Pinkerton and Stevenson, 1992; Harris and Allen, 2008; Chevrel et al., 2013; Mader et al., 2013; Truby et al., 2015; Dietterich et al., 2018a) or power-law fluids (Hardee and Dunn, 1981; Spera et al., 1988; Pinkerton and Norton, 1995; Sakimoto et al., 1997; Sonder et al., 2006; Piombo and Dragoni, 2009), the phenomenon occurs in channels in close proximity to the vent area, where high velocities, high discharge rates, high temperatures, low melt viscosities and crystal content justify this assumption (Dragoni et al., 1986; Pinkerton and Stevenson, 1992; Tallarico and Dragoni, 1999; Griffiths, 2000; Chevrel et al., 2019; Harris et al., 2020);
4. Shear along channel walls is neglected, implying a uniform velocity across the channel's cross-section area. As such, the average velocity is equal to the velocity at any point on the section. In Eq. (7), the kinetic energy correction factor becomes $\gamma \rightarrow 1$. This approximation is valid assuming a simple channel geometry (Chow, 1959) and as lava flows undergoing a hydraulic jump will have relatively low viscosities, limiting the shear zone width.
5. For a well-mixed channel, the density and apparent viscosity is uniform in the vertical z-axis (Tallarico and Dragoni, 1999; Robert et al., 2014).

6. The lava is considered as an incompressible fluid, even though lava flows may contain a non-negligible amount of gas bubbles near the vent.
7. It has been shown that lava may thermally erode the base of the lava channel at rates on the order of cm/day (Jarvis, 1995; Kauahikaua et al., 1998; Kerr, 2001; Siewert and Ferlito, 2008). However, over the short time period of an observation of a standing wave (~minutes to hours), we consider no channel bed erosion.

5.2. Flow Velocity and Discharge Rate

The length of the jump, L_j, and the height of the jump, A_j, are dependent on Fr_1 and H_1 (Chow, 1959; French, 1986; Chaudhry, 2008):

$$L_j = 220H_1 \times \tanh\left(\frac{Fr_1 - 1}{22}\right) \tag{11}$$

$$A_j = \frac{H_1\sqrt{1 + 8Fr_1^2} - 3H_1}{2} \tag{12}$$

where *tanh* is the hyperbolic tangent. These equations are valid for $Fr_1 < 4$ (Hager, 1992; Chaudhry, 2008). Thus, for a given L_j or A_j and H_1, we can calculate the Froude number of the flow. Using the definition of a critical flow (Eq. (7)), v_1 is estimated for a given channel slope by:

$$v_1 = Fr_1\sqrt{gH_1\cos\alpha} \tag{13}$$

Knowing the channel width, W, we obtain the discharge rate in m^3/s:

$$Q = v_1 \times H_1 \times W \tag{14}$$

Due to momentum conservation, Q is constant upstream and downstream of the hydraulic jump.

5.3. Lava flow depth

Knowing the lava flow velocity, v_1, the lava depth in the channel can be estimated from the amplitude of the hydraulic jump. This is obtained by combining Eqs. (7), (8), (12) and (13). Further details of the derivations are given in the Appendix C. The lava depth is calculated by:

$$H_1 = \frac{1}{2}H_C - \frac{1}{4}\left[\frac{3\omega A_j - \sqrt{\Omega}}{\omega}\right] \tag{15}$$

where, H_C is the critical depth as defined in Eq. (8), $\omega = g\cos\alpha$ and $\Omega = 4v_1^2(v_1^2 - 3\omega A_j) + (\omega A_j)^2$.

5.4. Lava apparent viscosity

To calculate the lava apparent viscosity, η, we use the expression of the Reynolds number as defined in Eq. (1). First, we must calculate *Re*, via the Fanning friction factor, *f*. *f* is a dimensionless factor that relates the friction loss on the channel walls to the flow's kinetic energy that is proportional to the flow's squared velocity (Chow, 1959; Burger et al., 2015; LaViolette, 2017). The Fanning friction factor is introduced by the shear stress, τ_s (N/m^2). τ_s is calculated based on the principle of momentum conservation balanced by the pressure drop (P_2-P_1, Fig. 7). It is a force at the fluid-channel boundary that measures the friction on the channel walls and base. τ_s follows (Hulme, 1974; Fink and Zimbelman, 1990; Osmond and Griffiths, 2001):

$$\tau_s = \rho g D \sin\alpha \tag{16}$$

where τ_s describes the drag force of a moving fluid along the channel boundaries and D is the hydraulic diameter. Therefore, related to the flow velocity:

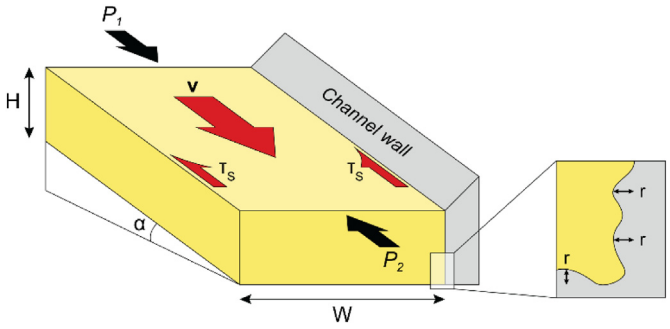

Fig. 7. Schematic diagram showing the different parameters influencing the Fanning friction factor, *f*, in a rectangular channel. τ_s is the shear stress along the channel side walls, *r* is the average height of the channel irregularities and P_1-P_2 is the pressure difference between two points of the channel.

$$\tau_s = \frac{f\rho v^2}{2} \tag{17}$$

f is a dimensionless parameter that depends on the flow velocity, *v*, *D*, and ρ. Rearranging Eqs. (16) and (17), *f* can be written as:

$$f = \frac{gD\sin\alpha}{2v^2} \tag{18}$$

In open channel hydraulics, the turbulent state of the flow is often expressed in a space representing the relationship *f* vs. *Re* (also referred to as the Stanton or Moody diagram; Fig. 8; Stanton and Pannell, 1914; Chow, 1959; Burger et al., 2015; LaViolette, 2017). Indeed, *f* is a function of *Re* and different relationships can be expressed between *Re* and *f*, depending on the nature of the flow (LaViolette, 2017). For $Re < 2000$, *f* is proportional to *Re* through the constant, *K*, such that:

$$f = \frac{K}{Re} \tag{19}$$

K is a purely numerical coefficient that depends on the channel shape and roughness of the channel walls. For smooth rectangular channels, $K = 24$; for rough rectangular channels, $24 < K < 60$ (Chow, 1959). These values of *K* were originally developed from compilations of the water hydraulic experimental datasets by Chow (1959). Nevertheless, it has been shown by Burger et al. (2010) and by the extensive experimental dataset of Burger et al. (2015) for different channel cross section shapes, that the relation *f*/*Re* for non-Newtonian flows closely follows the same trends as for Newtonian flows.

Lava flows with a turbulent behavior have been reported only a few times (Baloga et al., 1995). In turbulent conditions ($Re > 2000$), we can apply the Blasius equation, which is valid for $2000 < Re < 25{,}000$ for smooth channels (Blasius, 1912; Chow, 1959; LaViolette, 2017):

$$f = 0.079/\ Re^{0.25} \tag{20}$$

For rough channels, the formulation for turbulent flows is dependent on the average height of channel wall irregularities, *r* (m):

$$\frac{1}{\sqrt{f}} = 2\log\left(\frac{12\ Re}{r}\right) \tag{21}$$

Once *f* is calculated using Eq. (18), we can estimate *Re* using one of the *f*/*Re* equations described above depending on the channel conditions. The appropriate *f*/*Re* equation is determined when the value of *f* is plotted on the *f* vs. *Re* diagram (Fig. 8a). η is then derived from Eq. (1) for a given ρ.

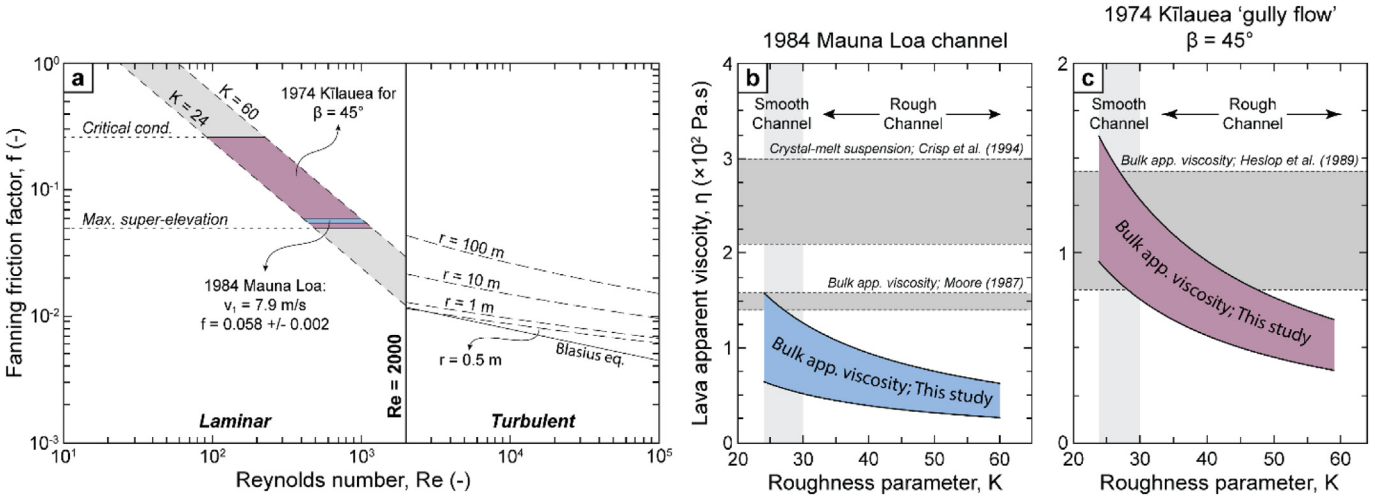

Fig. 8. Estimate of the Reynolds number, *Re*, and lava viscosity, η, of the 1984 Mauna Loa and 1974 Kīlauea gully flows. Results for 1974 Kīlauea gully are for $\beta = 45°$. See Table 2 for other values of β. (a) The *f* vs. *Re* diagram (Stanton and Pannell, 1914; Chow, 1959; Burger et al., 2015; LaViolette, 2017) allows the calculation of *Re* when *f* is known. In laminar conditions, *f* is related to *Re* by a roughness factor, *K* (Chow, 1959; Burger et al., 2010, 2015; LaViolette, 2017). The suggested value of *K* corresponds to smooth channels, $24 < K < 30$ (see text for more details). In turbulent conditions, *Re* follows the Blasius equation for smooth channels (Blasius, 1912; Chow, 1959; LaViolette, 2017). For rough channels, *Re* depends on the average height of the rough particles on the channel walls, *r* (see Fig. 7). (b and c) Roughness factor *K* vs. η for the 1984 Mauna Loa channel and 1974 Kīlauea '*gully flow*', respectively. η is estimated by Eq. (1) with *Re* values previously estimated from *f*. vs. *Re* diagram. For comparison, we have plotted in both cases the estimated viscosity ranges from previous studies.

5.5. Note on the channel roughness, K and r

As explained earlier, the lava apparent viscosity is obtained from the Reynolds Number, *Re*, via the Fanning friction factor, *f* and by the roughness parameter *K* in the laminar regime and *r* in the turbulent regime (Fig. 8). The roughness of a lava channel corresponds to the irregularities on the channel walls and floor. On channel walls, the roughness is mainly due to solidified lava from drainage of overflows back into the channel or channel wall accreted sheets (Harris et al., 2009). Roughness on the channel floor is usually due to lava ropes from previous solidified flows (Fink and Fletcher, 1978). These features are 1–10 cm high. With rectangular channels 1–10 m deep, the ratio of the average particle height to the channel depth is 1/10–1/100; channel roughness does not therefore play a significant role in the lava flow dynamics. For a basaltic lava flow with viscosity in the range of 10^2–10^3 Pa.s (eruptive viscosity for most of the basaltic lava flows on Earth), the lava is generally in a laminar regime or in the transitional regime even for high speed flows. For laminar regimes, Eq. (19) can be therefore used with a suggested value of $K < 30$ (i.e., ~smooth channel). However, changes in the value of *K* will have a very limited effect on the deduced viscosity. For a given lava density, there is a maximum difference ~75 Pa·s between $K = 24$ and $K = 60$ (Fig. 8).

The turbulent regime may only be reached with extremely high velocities or for a particular lava composition such as carbonatite or komatiite (e.g., Huppert et al., 1984; Baloga et al., 1995; Jarvis, 1995). For $r < 0.5$ m, the Blasius equation (Eq. (20)) and Eq. (21) give similar approximation of the Reynolds number for $2000 < Re < 10^4$ (Fig. 8). In the case of extremely fast lava flows, i.e., $v > 20$ m/s, the roughness parameter becomes critical in the estimation of the Reynolds number and the resulting lava apparent viscosity.

6. Application to an active and a drained lava channel

6.1. 1984 Mauna Loa Channel

The assessment of channel depth on active lava flows is challenging, but crucial for the estimation of discharge rates and hazard assessment. For a lava flow under supercritical conditions and exhibiting an undular hydraulic jump, the channel depth can be calculated by Eq. (15) (see details in Appendix C). We use the 1984 Mauna Loa eruption to demonstrate the method. This estimation of flow depth allows us to calculate the channel discharge rate and lava apparent viscosity.

6.1.1. Lava channel and standing wave descriptions

We used the video segment from the "*Into the Inferno*" movie (Herzog, 2016) as it has the best available quality of these standing waves (Fig. 9a). We scaled the video based on the volcanologist shown observing the nearby standing waves. We assumed a height of 1.77 m for the volcanologist which is the average height of a person living in the U.S.A. (Ogden et al., 2004). Using this, we estimate a channel width of 7–8 m, a jump of ~15 m in length and about 1.9 m high (Fig. 9a). Downstream of the first wave, there are several stationary surface waves. The waves do not have rollers. Lateral shockwaves are observed from the channel sidewalls but have smaller amplitudes than the waves in the channel centre line. These observations are characteristic of a non-breaking undular jump as described by Ohtsu et al. (2003) (Appendix A). Therefore, we might expect Fr_1 in the range of 1 to $Fr_{1,limit}$, with $Fr_{1,limit} < 4$ (Appendix A; Ohtsu et al., 2003; Chanson, 2009).

6.1.2. Lava flow dynamics

Using velocimetry analysis of the video, we calculate a maximum surface velocity of ~7.9 m/s at the centre of the channel just upstream of the standing wave (Fig. 9b). The surface velocity was estimated using an implementation of a classic Optical Flow algorithm (Horn and Schunk, 1981) including modern modifications (Sun et al., 2010) used to study lava flows (Lev et al., 2012). With an upstream flow velocity of $v_1 = 7.9$ m/s (Fig. 9b), the critical lava flow depth is $H_c = 6.4$ m (Eq. (8)). Therefore, H_1 should be lower than H_c in order to have a lava in supercritical state and exhibit a hydraulic jump. The upstream flow depth of a lava exhibiting an undular hydraulic jump is given by Eq. (15) and using $A_j = 1.9$ m, we estimate $H_1 = 2.8$ m. The corresponding Froude number is $Fr_1 = 1.48$. As a comparison, Lipman and Banks (1987) estimated a channel depth of 3 m near the vent. Our results give a discharge rate of $Q = 171 \pm 12$ m^3/s. Upstream of the jump, the channel cross-section is $A = 21.7 \pm 1.5$ m^2, the wetted perimeter $P_W = 13.3 \pm 0.5$ m and the hydraulic diameter $D = 6.5 \pm 0.2$ m. Using Eq. (18), $f = 0.058 \pm 0.002$ (Fig. 8a). From the *f* vs. *Re* diagram, the lava flow is in a laminar state, and for $24 < K < 30$, $Re = 468 \pm 68$.

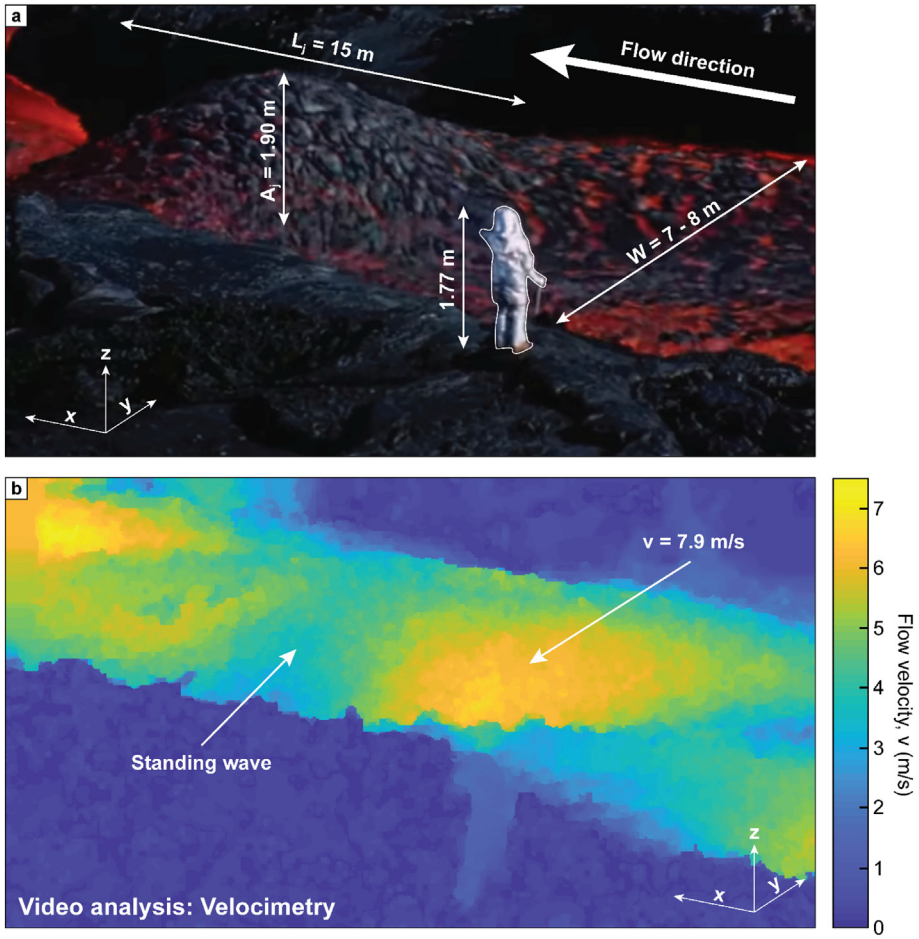

Fig. 9. Standing wave in a 1984 Mauna Loa lava channel. (a) Screenshot from the film "*Into the Inferno*" by Herzog (2016). (b) Velocimetry showing the lava flow speed in the region of the standing wave.

Finally, with $\rho = 910 \pm 260$ kg/m^3 (~55–75 vol% of vesicles; Lipman and Banks, 1987; Moore, 1987), the lava bulk apparent viscosity, $\eta = 107 \pm 47$ Pa·s (Fig. 8b). This compares with the ~140–160 Pa·s calculated by Moore (1987) after direct observation of the channelized lava from April 2 to April 6, 1984. From petrological analyses of a lava sample collected near the vent on April 2, Crisp et al. (1994) estimated a viscosity of 255 ± 45 Pa·s for the crystal-melt suspension. The difference with our calculations is explained by the fact that bubbles in high speed lava channels must be elongated which tends to lower the bulk viscosity of the lava flow (e.g., Llewellin and Manga, 2005; Mader et al., 2013).

6.2. 1974 Kīlauea 'Gully Flow'

Heslop et al. (1989) suggested that a supercritical lava flow could have been responsible for the raised levees on the outer gully wall (Fig. 10). In this situation, we suggest that an oblique hydraulic jump (similar to Fig. 4) may have been responsible for the formation of the super-elevated levees. As in straight lava channels, several super-elevated lava levels are preserved. These elevation changes correspond to variations of the lava discharge rate in the channel. Elevation of the levees indicates an increase of the discharge rate, whereas decline of the lava level shows decrease of the discharge rate. The aim is to estimate a range of velocities, v_1, discharge rates, Q, and apparent viscosities, η, that could have formed the super-elevation of lava levees at the channel bend. In the calculations below, we estimate these lava flow conditions at (1) the critical conditions and (2) when the maximum elevation of the levees, i.e., 3.15 m above the average flow depth, are reached. Results of the later will correspond to the flow conditions when the lava discharge rate was maximum.

6.2.1. Geometry at the channel bend

The channel geometry is similar to the one presented in Fig. 4. Our inputs are the channel depth, $H_1 = 3.35$ m, channel width, $W = 8$ m, underlying slope, $\alpha = 7.5°$, channel bend, $\theta = 45°$ and lava density, $\rho = 875 \pm 225$ kg/m^3 (obtained from 4 lava samples collected in the channel; Heslop et al., 1989). Immediately upstream of the oblique hydraulic jump, the channel cross section is $A = 26.8$ m^2, the wetted perimeter, $P_W = 14.7$ m and the hydraulic diameter, $D = 7.3$ m (Eqs. (2) and (3)). The angle, β, of the oblique hydraulic jump wavefront with the original gully wall direction is unknown. However, β should be between 45° and 90° (Fig. 11). H_2 is also unknown, however, it should be higher than H_1 and lower than the maximum super-elevation of the levees, i.e., $3.35 < H_2 < 6.5$ m. Therefore, we have $(H_2/H_1)_{max} = 1.94$.

6.2.2. Lava flow conditions at critical state

The critical conditions, i.e., $Fr_1 = 1$ are reached when $v_1 = 5.71$ m/s (Eq. (7)). This corresponds to $Q = 153$ m^3/s. From Eq. (18), $f = 0.143$. Using the f vs. Re diagram (Fig. 8a), we have $Re < 2000$ indicating laminar conditions at the critical state (unless, $r > 10$ m, which is not applicable for this flow). Therefore, with $24 < K < 30$, $Re = 188 \pm 20$ and the lava apparent viscosity is $\eta = 200 \pm 71$ Pa·s.

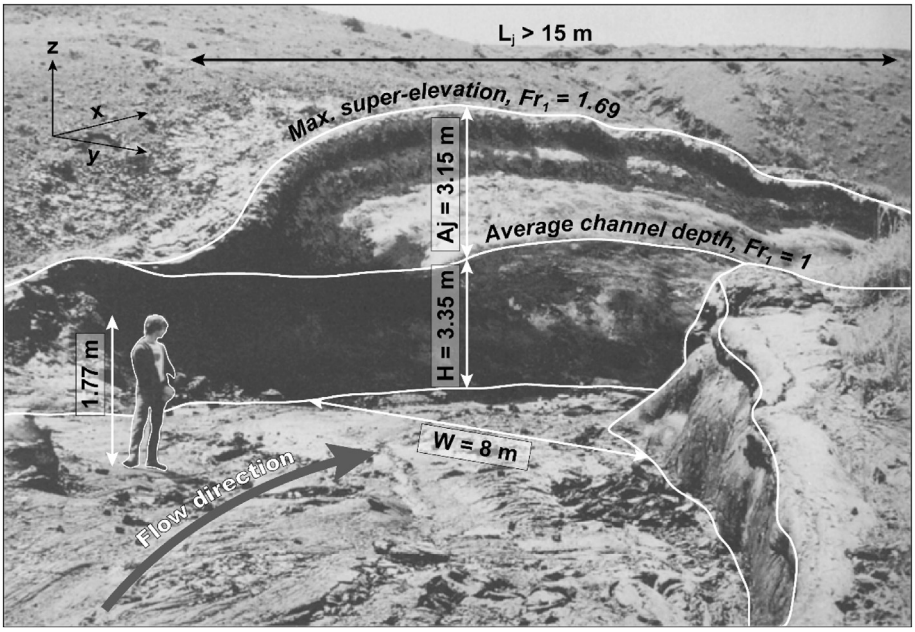

Fig. 10. Super-elevated levees at channel bend number 3 of the 1974 Kīlauea '*gully flow*', modified from Heslop et al. (1989). The bend angle is $\theta = 45°$. This feature was formed by an oblique hydraulic jump at this channel bend indicating lava under supercritical conditions. The maximum super-elevation of $A_j = 3.15$ m above the average flow depth. The wavefront angle, β, is unknown but should be $\theta < \beta < 90°$. The maximum super-elevation corresponds to Froude number of 1.69 (Fig. 11) that gives a maximum lava flow velocity of 9.65 m/s.

6.2.3. Lava flow conditions in supercritical state

Fig. 11 shows the range of Froude number that satisfies Eq. (A.3) for an oblique jump given the above inputs. We find a maximum upstream Froude number of 1.69 for $\beta = 45°$ and $(H_2/H_1)_{max}$. As a comparison, Lev et al. (2012) estimated $Fr = 1.6$ for the same flow. This corresponds to a maximum upstream velocity of $v_1 = 9.65$ m/s that gives $Q = 259$ m^3/s (Eqs. (13), (14)). From Eq. (18), $f = 0.050$ and $Re < 2000$ according to the f vs. Re diagram for whichever f/Re curves (Fig. 8a). Therefore, even during the maximum discharge rate, the lava flow was still under a laminar state. With $24 < K < 30$, $Re = 540 \pm 60$ (Lev et al. (2012) gave $Re = 586$) resulting in $\eta = 118 \pm 42$ Pa.s (Fig. 8c). These values compare well with the 85–140 Pa·s calculated by Heslop et al. (1989) (Fig. 8). Table 2 shows the lava flow conditions for wavefront angles of $\beta = 50°$, 60°, 70° and 80°. By increasing the wavefront angle, the upstream flow velocity decreases as does the discharge rate leading to slightly higher viscosities.

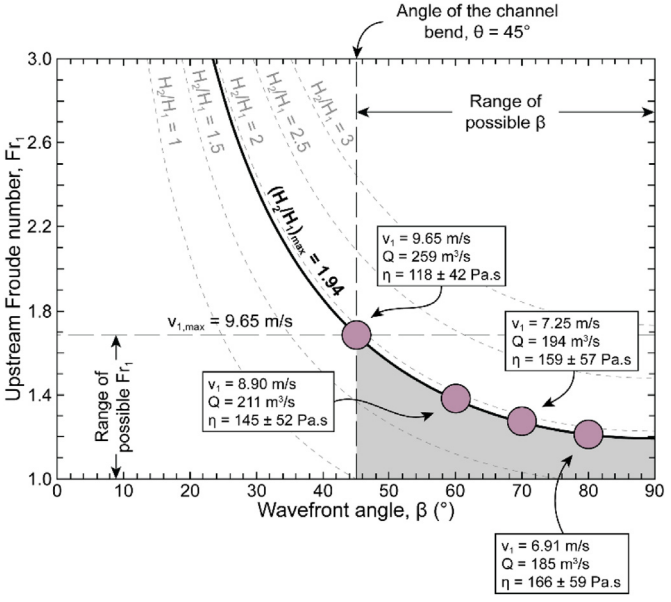

Fig. 11. In grey, conditions (Fr_1 and β) that satisfy the equation of the oblique hydraulic jump (Eq. (A.3)) for the super-elevated levees in the 1974 Kīlauea '*gully flow*' at bend number 3. $(H_2/H_1)_{max}$ corresponds to the maximum super-elevation with $H_1 = 3.35$ m. The purple circles show the possible apparent lava viscosity, discharge rate and upstream velocity for the formation of the maximum super-elevation for $\beta = 45°$, 60°, 70° and 80°.

7. Discussion, summary and perspectives

A number of channelized lava flows exhibiting standing waves have been reported in historical lava flows (Appendix B). This phenomenon generally occurs in close proximity to the vent area, at relatively high speeds, and is usually located at a break in slope or at channel bends; they are sometimes directly referred to as hydraulic jumps. Importantly, this phenomenon indicates lava flow under supercritical conditions and therefore, assuming Newtonian flow, we can apply open channel hydraulics theory to supercritical flow in order to extract several key parameters in flow dynamics. The flow depth, velocity and discharge rate are calculated using the Froude Number, the length and amplitude of the standing waves. Combining the Fanning friction factor and the Reynolds number we can determine the apparent viscosity of the lava flow.

7.1. Flow regime in lava channels

As noted above, the critical state of a flow is given by the Froude Number, Fr, and reflects the effect of gravity on the flow dynamics. The turbulence state of the flow is given by the Reynolds Number, Re and is related to the effect of viscosity on flow movement. Thus, the two parameters define four possible combinations of flow regimes (Fig. 12). Hydraulic jumps occur:

- when $Fr > 1$ and $Re < 2000$, the flow is in a supercritical-laminar state;
- when $Fr > 1$ and $Re > 2000$, the flow is in a supercritical-turbulent state.

Table 2
Lava flow conditions for the formation of the maximum super-elevated levees in the 1974 Kīlauea 'gully flow', for different wavefront angle. *Re* and η are calculated for $24 < K < 30$.

Wavefront angle, β (°)	Upstream Froude number, Fr_1	Upstream velocity, v_1 (m/s)	Discharge rate, Q (m^3/s)	Fanning friction factor, *f*	Reynolds number, *Re*	Apparent viscosity, η (Pa·s)
45	1.69	9.65	259	0.050	540 ± 60	118 ± 42
50	1.56	8.90	239	0.059	457 ± 50	129 ± 46
60	1.38	7.88	211	0.075	360 ± 40	145 ± 52
70	1.27	7.25	194	0.089	303 ± 33	159 ± 57
80	1.21	6.91	185	0.098	275 ± 30	166 ± 59

We estimate the potential flow regimes in the 1984 Mauna Loa (Fig. 12a, c) and 1974 Kīlauea gully (Fig. 12b, d)channels by examining a range of possible lava and flow parameters. The flow regimes presented here correspond to the conditions just upstream of the standing wave. We vary η between 10 and 500 Pa.s and H_1 from ~0.25 to 20 m. For reference, the results obtained in the above sections for the

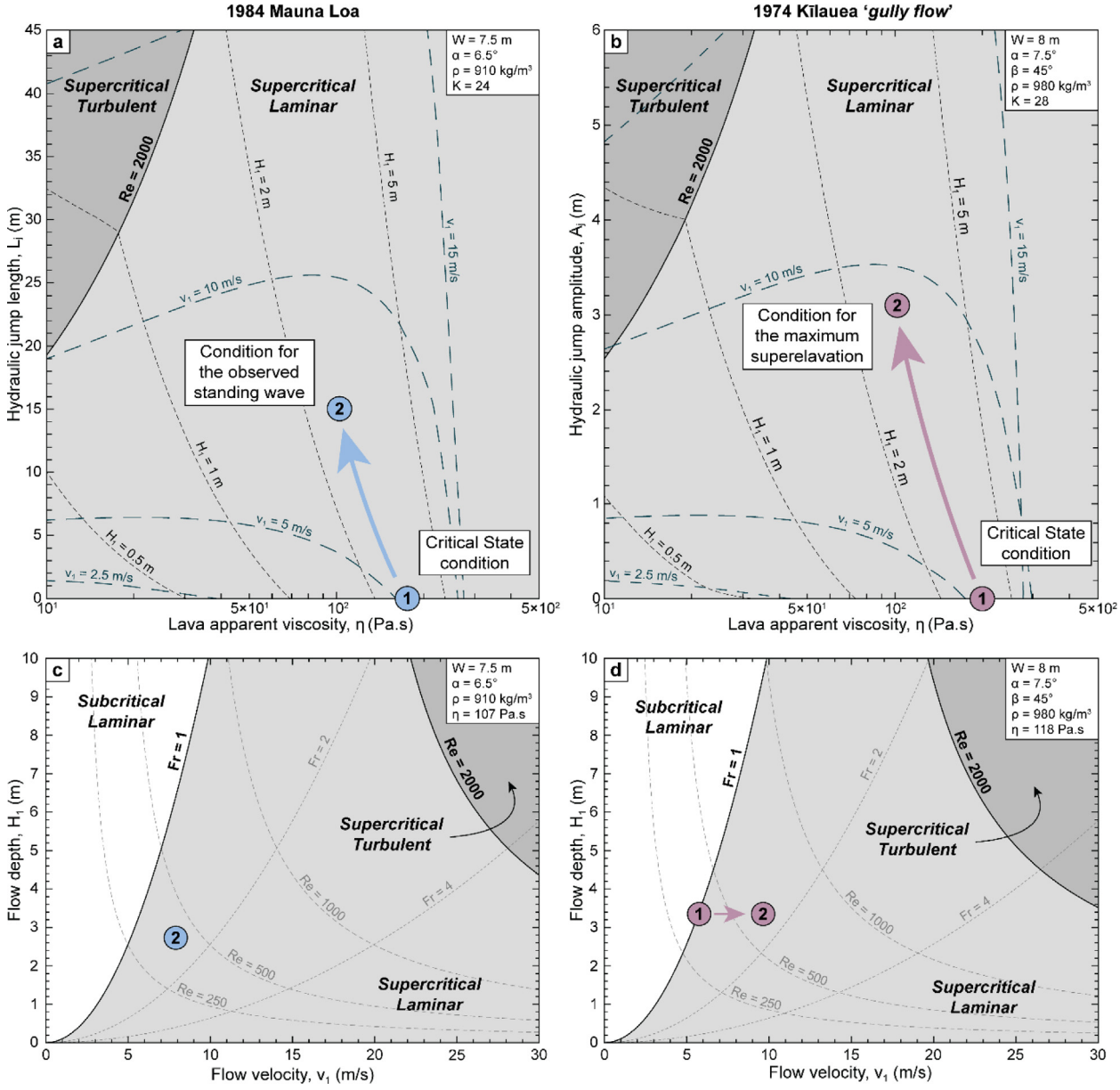

Fig. 12. Flow regimes for the 1984 Mauna Loa channel and the 1974 Kīlauea '*gully flow*' upstream of the hydraulic jumps. The 1984 Mauna Loa flow regimes are calculated assuming $W = 7.5$ m, $\alpha = 6.5°$, $K = 24$, $\rho = 910$ kg/m^3. The 1974 Kīlauea flow regimes are calculated assuming $W = 8$ m, $\alpha = 7.5°$, $\beta = 45°$, $K = 28$, $\rho = 980$ kg/m^3. The *Re* curves denote the transition from laminar to turbulent. The $Fr = 1$ curves denote the transition from subcritical to supercritical condition. (a, b) Lava viscosity, η is plotted as a function of L_j for the Mauna Loa channel and A_j for the 1974 Kīlauea '*gully flow*'. (c, d) The flow regimes are represented in a space v_1 vs. H_1. We use $\eta = 107$ Pa·s and 118 Pa·s for the 1984 Mauna Loa channel and 1974 Kīlauea '*gully flow*', respectively. The purple and blue markers represent the lava flow conditions: (1) critical state; (2) conditions of the observed standing wave (1984 Mauna Loa) or conditions for the maximum super-elevation of the levees (1974 Kīlauea '*gully flow*'). In (c), the critical conditions are unknown (they could be anywhere on the $Fr = 1$ curve).

two case studies are shown. Hydraulic jumps in lava flow become possible when:

- the lava is channelized (Figs. 3, 4, 6);
- the velocity head ($v^2/2g$) is larger than half pressure head ($H \cos \alpha$) (Fig. 2; Eqs. (5), (6)). For example, the velocity head in the 1984 Mauna Loa channel before the observed standing wave is ~1.13 times greater than the pressure head;
- $v_1 > 2.5$ m/s (for $\eta \approx 10$–50 Pa·s and $H_1 < 0.5$ m) to $v_1 \approx 15$ m/s (for $\eta \approx 300$–400 Pa·s and $H_1 \approx 6$ m; Fig. 12).

It is not possible to have a supercritical flow, and therefore a hydraulic jump, for $\eta > 500$ Pa·s, unless $v_1 > 20$ m/s and $H_1 > 20$ m; this is unlikely to occur for basaltic lava flows on Earth. The turbulence state in supercritical conditions corresponds to $\eta < 100$ Pa.s and $v_1 > 7$ m/s for $L_j > 10$ m or $A_j > 2.5$ m and $H_1 \approx 0.25$–3 m. This regime may have been reached by very low viscosity and channelized lavas such as komatiite flows (Huppert and Sparks, 1985; Williams et al., 1998).

7.2. Accurate calculation of flow depth and discharge rates in high speed lava channels

Accurate assessment of flow velocity and channel depth are critical input parameters in deterministic lava flow modelling used for hazard mitigation during volcanic crises (Harris and Rowland, 2001; Costa and Macedonio, 2005; Hidaka et al., 2005; Cordonnier et al., 2016; Fujita and Nagai, 2016; Kelfoun and Vargas, 2016). Identifying standing waves in active lava channels can be an important tool to enable real time and precise monitoring of lava flow dynamics in the near vent area (Fig. 13). Furthermore, the discharge rate of a channelized lava can be calculated from measurements of flow velocity, channel width and depth. While flow velocity and channel width can be estimated from video analysis (e.g., velocimetry), channel depth of an active lava flow is extremely difficult to estimate and is thus one of the greatest sources of error (Lev and James, 2014). For example, overestimation of channel depth by only 1 m for the 1984 Mauna Loa example would have resulted in a ~40% greater discharge rate estimate. Fortunately, real-time video surveys of active lava flows are becoming standard thanks to the rapid advance of ground based video acquisition and Uncrewed Aerial Vehicles (UAV) technology (e.g., Lev et al., 2012, 2018; Dietterich et al., 2018b; Patrick et al., 2019; James et al., 2020). If standing waves are identified in such videos, the channel depth can be rapidly calculated with precision from the amplitude and/or length of the standing waves (via the Froude number) using the methodology presented here; in conjunction with velocity and channel width measurements from the video, this can provide accurate discharge rates (Fig. 13).

7.3. Reconstruction of the flow dynamics of historical lava flows

In addition to its clear benefit for monitoring flow conditions during an active eruptive crisis, the analysis of standing waves preserved in the channels of past flows can also be applied to reconstruct lava flow dynamics of historical lava, as we demonstrate through the 1974 Kīlauea '*gully flow*'. By applying the same methodology, the dynamics of past lava flows can be determined in other locations where standing waves have been preserved in the lava deposits. For example, super-elevated levees at channel bends similar to those in the 1974 Kīlauea gully are present in a confined lava channel near Pico Partido volcano, Lanzarote Island, Canary Islands (Woodcock, 2003; Woodcock and Harris, 2006). While the lack of data limits proper assessment of the lava flow properties in this channel, a high velocity flow in a supercritical state was suggested; Woodcock (2003) calculated a Froude number of 2.3 and 2.9 at two different channel bends (Appendix B). Similar morphological features may also be present in other historical high speed lava flows such as the 1801 Hualalai lava channel (Hawai'i), or the 1823 Keaiwa lava flow (Kīlauea; Baloga et al., 1995; Guest et al., 1995) where the 11 m super-elevated lava deposits (called the '*plastered cones*') may have resulted from an oblique standing wave (similar to Fig. 4). Investigating such morphological features can greatly improve our understanding of the emplacement and dynamics of these lava flows and requires high resolution topographic mapping of the channels and, where possible, direct measurements of super-elevated levees dimensions.

8. Conclusions

Standing waves in a lava channel were identified as the result of lava flow in supercritical conditions. Standing waves generally occur in high speed channels and in close proximity to the vent. Therefore, assuming the lava can be approximated as a Newtonian fluid, open channel hydraulic theory allows the calculation of channel depth, velocity and discharge rate using the length and amplitude of the standing waves via the Froude number. The lava apparent viscosity is estimated using the Reynolds number. Here, we present a methodology that estimates those parameters, critical in lava flow modelling. Our results are in good agreement with historical data for two examples from Hawai'i; we reproduce past measurements using channel deposit geometry (for the 1974 Kīlauea '*gully flow*',) and video analysis (for the 1984 Mauna Loa channel). Therefore, standing waves could be used to reconstruct the dynamics of historical lava flows. With the rapid advance in video acquisition in the field during eruptions, scientists can deploy low cost equipment near open lava channels in order to monitor the lava channel evolution and flow discharge rate. Identifying standing waves in an active open lava channel allows rapid determination of

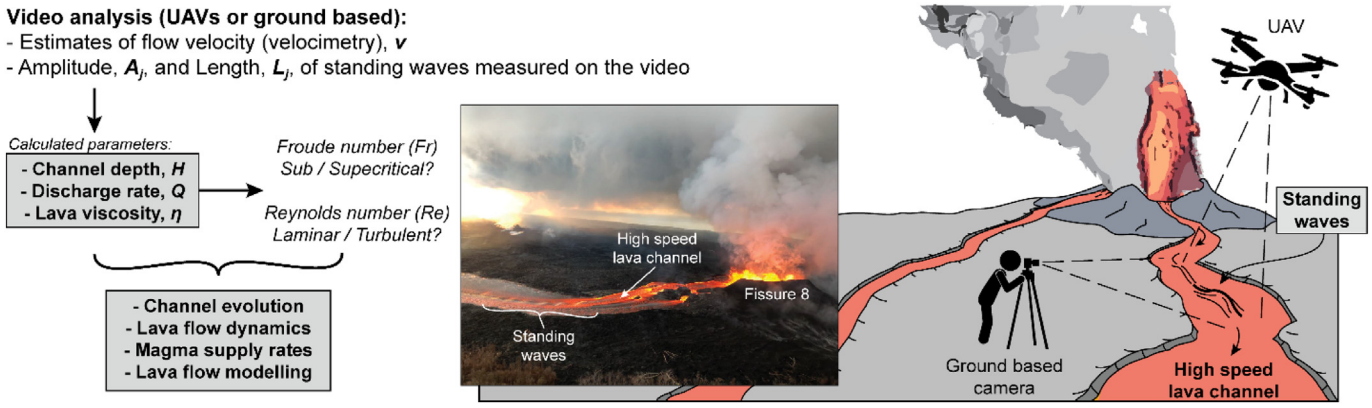

Fig. 13. Methodology for calculation of channel depth, discharge rate and lava viscosity in order to determine the lava flow regime (*Fr* and *Re* numbers) from UAV or ground based acquired video when a standing wave is present at spillways. Inset: photo of the Fissure 8 lava channel (USGS, Hawaiian Volcano Observatory, June 13, 2018). Standing waves are present in the middle of the high speed lava channel, about 200 m from the vent. Preliminary estimate of the velocity is up to 15 m/s (Patrick et al., 2019).

the channel depth, discharge rate and lava apparent viscosity, critical parameters in monitoring an ongoing eruption (Fig. 13). While some of the assumptions in this work may seem too restrictive, this can be easily applied to all active and well monitored volcanoes where high-speed lava flows have been historically observed and where a potential threat to the local communities and human infrastructure exists (e.g., Kīlauea, Mauna Loa, Sierra Negra, Piton de La Fournaise, Nyiragongo, etc.). This can be a powerful yet simple tool to assess the evolution of lava channels, lava flow dynamics and magma supply rates.

Supplementary data to this article can be found online at https://doi.org/10.1016/j.jvolgeores.2020.106944.

CRediT authorship contribution statement

Y. Le Moigne: Conceptualization, Methodology, Investigation, Writing - original draft, Writing - review & editing, Supervision, Visualization.**J.M. Zurek:**Conceptualization, Writing - original draft, Writing - review & editing.**G. Williams-Jones:**Writing - original draft, Writing - review & editing, Supervision, Funding acquisition.**E. Lev:**Conceptualization, Methodology, Writing - original draft.**A. Calahorrano-Di Patre:** Conceptualization, Methodology, Writing - original draft, Writing - review & editing.**J. Anzieta:**Conceptualization, Methodology, Writing - review & editing.

Declaration of competing interest

The authors declare that they have no known competing financial interests or personal relationships that could have appeared to influence the work reported in this paper.

Acknowledgments

The authors greatly appreciate the thorough comments from Jonathan Fink and Kelly Russell. We acknowledge the constructive reviews of G. Grant, S. Kolzenburg and L. Keszthelyi.

Funding

This work is supported by a Natural Sciences and Engineering Research Council of Canada Discovery grant to GWJ and Simon Fraser University Research scholarship to YLM.

Author contributions

YLM, JMZ, GWJ, ACDP and JA conceptualized the idea that hydraulic jumps in high speed lava channels can be used to provide eruption parameters. YLM compiled the data from the literature, applied hydraulic theory for supercritical flows to lava channels, prepared and created the data presentation. EL performed velocimetry calculations on the 1984 Mauna Loa lava channel video. All the authors contributed to the writing of the manuscript.

Data and materials availability

Data access information and additional methodologies are provided in the manuscript or in supplementary materials.

References

Alexander, J., Bridge, J.S., Cheel, R.J., Leclair, S.F., 2001. Bedforms and associated sedimentary structures formed under supercritical water flows over aggrading sand beds. Sedimentology 48, 133–152. https://doi.org/10.1046/j.1365-3091.2001.00357.x.

Balmforth, N.J., Burbidge, A.S., Craster, R.V., Salzig, J., Shen, A., 2000. Visco-plastic models of isothermal lava domes. J. Fluid Mech. 403, 37–65. https://doi.org/10.1017/S0022112099006916.

Baloga, S.M., Spudis, P.D., Guest, J.E., 1995. The dynamics of rapidly emplaced terrestrial lava flows and implications for planetary volcanism. J. Geophys. Res. Solid Earth 100, 24509–24519. https://doi.org/10.1029/95JB02844.

Behncke, B., Neri, M., Nagay, A., 2005. Lava flow hazard at Mount Etna (Italy): New data from a GIS-based study. In: Manga, M., Ventura, G. (Eds.), Kinematics and dynamics of lava flows 396. Geol. Soc. Am. Spec. Pap., pp. 189–208.. https://doi.org/10.1130/0-8137-2396-5.189.

Blasius, H., 1912. Das Aehnlichkeitsgesetz bei Reibungsvorgängren. Z. Ver. Dtsch. Ing. 56, 639–643.

Bradley, J.N., Peterka, A.J., 1957. The hydraulic design of stilling basins: hydraulic jumps on a horizontal apron (basin I). Proc. ASCE, J. Hydraul. Div. 83, 1–24.

Burger, J., Haldenwang, R., Alderman, N., 2010. Experimental database for non-Newtonian flow in four channel shapes. J. Hydraul. Res. 48, 363–370. https://doi.org/10.1080/00221686.2010.481849.

Burger, J.H., Haldenwang, R., Alderman, N.J., 2015. Laminar and turbulent flow of non-newtonian fluids in open channels for different cross-sectional shapes. J. Hydraul. Eng. 141. https://doi.org/10.1061/(ASCE)HY.1943-7900.0000968.

Cartigny, M.J.B., Ventra, D., Postma, G., van Den Berg, J.H., 2014. Morphodynamics and sedimentary structures of bedforms under supercritical-flow conditions: new insights from flume experiments. Sedimentology 61, 712–748. https://doi.org/10.1111/sed.12076.

Cashman, K.V., Mangan, M.T., 2014. A century of studying effusive eruptions in Hawai'i. In: Poland, M.P., Takahashi, T.J., Landowski, C.M. (Eds.), Characteristics of Hawaiian Volcanoes. U.S. Geol. Surv. Prof. Paper 1801, pp. 357–394. https://doi.org/10.3133/pp1801.

Cashman, K.V., Mangan, M.T., Newman, S., 1994. Surface degassing and modifications to vesicle size distributions in active basalt flows. J. Volcanol. Geotherm. Res. 61, 45–68. https://doi.org/10.1016/0377-0273(94)00015-8.

Cashman, K.V., Soule, S.A., Mackey, B.H., Deligne, N.I., Deardorff, N.D., Dietterich, H.R., 2013. How lava flows: new insights from applications of lidar technologies to lava flow studies. Geosphere 9, 1664–1680. https://doi.org/10.1130/GES00706.1.

Cashman, K.V., Grant, G., Dietterich, H.R., Major, J.J., 2018. Implications of critical flow phenomena for estimating lava flux during recent activity at Kīlauea Volcano. American Geophysical Union Fall Meeting Abstracts (Washington, D. C).

Chanson, H., 2004. Environmental Hydraulics for Open Channel Flows. Elsevier Butterworth-Heinemann, Oxford.

Chanson, H., 2009. Current knowledge in hydraulic jumps and related phenomena. A survey of experimental results. Eur. J. Mech. B/Fluids 28, 191–210. https://doi.org/10.1016/j.euromechflu.2008.06.004.

Chaudhry, M.H., 2008. Open-channel Flow. Second Ed. Springer.

Chevrel, M.O., Platz, T., Hauber, E., Baratoux, D., Dingwell, D.B., 2013. Lava flow rheology: A comparison of morphological and petrological methods. Earth Planet. Sci. Lett. 384, 109–120. https://doi.org/10.1016/j.epsl.2013.09.022.

Chevrel, M.O., Harris, A.J.L., James, M.R., Calabrò, L., Gurioli, L., Pinkerton, H., 2018. The viscosity of pāhoehoe lava: in situ syn-eruptive measurements from Kilauea, Hawaii. Earth Planet. Sci. Lett. 493, 161–171. https://doi.org/10.1016/j.epsl.2018.04.028.

Chevrel, M.O., Pinkerton, H., Harris, A.J.L., 2019. Measuring the viscosity of lava in the field: a review. Earth-Science Rev. 196. https://doi.org/10.1016/j.earscirev.2019.04.024.

Chow, V.T., 1959. Open-channel Hydraulics. McGraw-Hill, New York doi: ISBN 07-010776-9.

Cole, P.D., Calder, E.S., Druitt, T.H., Hoblitt, R., Robertson, R., Sparks, R.S.J., 1998. Pyroclastic flows generated by gravitational instability of the 1996–97 lava dome of Soufriere Hills Volcano, Montserrat. Geophys. Res. Lett. 25, 3425–3428. https://doi.org/10.1029/98GL01510.

Comiti, F., Lenzi, M.A., 2006. Dimensions of standing waves at steps in mountain rivers. Water Resour. Res. 42, 1–13. https://doi.org/10.1029/2004WR003898.

Cordonnier, B., Lev, E., Garel, F., 2016. Benchmarking lava-flow models. Geol. Soc. Lond. Spec. Publ. 426, 425–445. https://doi.org/10.1144/SP426.7.

Costa, A., Macedonio, G., 2005. Numerical simulation of lava flows based on depth-averaged equations. Geophys. Res. Lett. 32, 1–5. https://doi.org/10.1029/2004GL021817.

Crisci, G.M., Iovine, G., Di Gregorio, S., Lupiano, V., 2008. Lava-flow hazard on the SE flank of Mt. Etna (Southern Italy). J. Volcanol. Geotherm. Res. 177, 778–796. https://doi.org/10.1016/j.jvolgeores.2008.01.041.

Crisp, J., Cashman, K.V., Bonini, J.A., Hougen, S.B., Pieri, D.C., 1994. Crystallization history of the 1984 Mauna Loa lava flow. J. Geophys. Res. Solid Earth 99, 7177–7198. https://doi.org/10.1029/93JB02973.

Dietterich, H.R., Downs, D.T., Stelten, M.E., Zahran, H., 2018a. Reconstructing lava flow emplacement histories with rheological and morphological analyses: the Harrat Rahat volcanic field, Kingdom of Saudi Arabia. Bull. Volcanol. 80. https://doi.org/10.1007/s00445-018-1259-4.

Dietterich, H.R., Patrick, M.R., Diefenbach, A.K., Parcheta, C., Lev, E., Foks, N.L., 2018. Lava flow hazard modeling and the assessment of effusion rates and topographic change with UAS and lidar during the 2018 Kīlauea lower East Rift Zone eruption. American Geophysical Union Fall Meeting Abstracts.

Dragoni, M., Bonafede, M., Boschi, E., 1986. Downslope flow models of a Bingham liquid: implications for lava flows. J. Volcanol. Geotherm. Res. 30, 305–325. https://doi.org/10.1016/0377-0273(86)90059-4.

Duller, R.A., Mountney, N.P., Russell, A.J., Cassidy, N.C., 2008. Architectural analysis of a volcaniclastic jökulhlaup deposit, southern Iceland: sedimentary evidence for supercritical flow. Sedimentology 55, 939–964. https://doi.org/10.1111/j.1365-3091.2007.00931.x.

Favalli, M., Chirico, G.D., Papale, P., Pareschi, M.T., Boschi, E., 2009. Lava flow hazard at Nyiragongo volcano, D.R.C. 1. Model calibration and hazard mapping. Bull. Volcanol. 71, 363–374. https://doi.org/10.1007/s00445-008-0233-y.

Field, W.G., Lambert, M.F., Williams, B.J., 1998. Energy and momentum in one dimensional open channel flow. J. Hydraul. Res. 36, 29–42. https://doi.org/10.1080/00221689809498375.
Finch, R.H., MacDonald, G.A., 1953. Hawaiian volcanoes during 1950. U.S. Geol. Surv. Bull. 996, 27–89. https://doi.org/10.3133/b996B.
Fink, J.H., Fletcher, R.C., 1978. Ropy pahoehoe: surface folding of a viscous fluid. J. Volcanol. Geotherm. Res. 4, 151–170. https://doi.org/10.1016/0377-0273(78)90034-3.
Fink, J.H., Zimbelman, J., 1990. Longitudinal variations in rheological properties of lavas: Puu Oo basalt flows, Kilauea Volcano, Hawaii. Lava Flows and Domes. Springer Berlin Heidelberg, pp. 157–173. https://doi.org/10.1007/978-3-642-74379-5_7.
Fralick, P., 1999. Paleohydraulics of chute-and-pool structures in a paleoproterozoic fluvial sandstone. Sediment. Geol. 125, 129–134. https://doi.org/10.1016/S0037-0738(99)00013-5.
French, R.H., 1986. Open-channel Hydraulics. McGraw-Hill Book Company.
Freundt, A., Schmincke, H.-U., 1985. Lithic-enriched segregation bodies in pyroclastic flow deposit of Laacher See Volcano (East Eifel, Germany). J. Volcanol. Geotherm. Res. 25, 193–224. https://doi.org/10.1016/0377-0273(85)90013-7.
Fujita, E., Nagai, M., 2016. LavaSIM: its physical basis and applicability. Geol. Soc. Lond. Spec. Publ. 426, 375–386. https://doi.org/10.1144/sp426.14.
Geist, D.J., Harpp, K.S., Naumann, T.R., Poland, M., Chadwick, W.W., Hall, M., Rader, E., 2008. The 2005 eruption of Sierra Negra volcano, Galápagos, Ecuador. Bull. Volcanol. 70, 655–673. https://doi.org/10.1007/s00445-007-0160-3.
Griffiths, R.W., 2000. The dynamics of lava flows. Annu. Rev. Fluid Mech. 32, 477–518. https://doi.org/10.1146/annurev.fluid.32.1.477.
Griggs, J.D., 1984. Mauna Loa Lava Flow, April 2, 1984. USGS, Mauna Loa Volcano, HI, US.
Guest, J.E., Spudis, P.D., Greeley, R., Taylor, G.J., Baloga, S.M., 1995. Emplacement of xenolith nodules in the Kaupulehu lava flow, Hualalai Volcano, Hawaii. Bull. Volcanol. 57, 179–184. https://doi.org/10.1007/BF00265037.
Guilbaud, M., Self, S., Thordarson, T., Blake, S., 2005. Morphology, surface structures, and emplacement of lavas produced by Laki, A.D. 1783–1784. Geol. Soc. Am. Spec. Pap. 396, 81–102. https://doi.org/10.1130/2005.2396(07).
Hager, W.H., 1985. Critical flow condition in open channel hydraulics. Acta Mech. 54, 157–179. https://doi.org/10.1007/BF01184843.
Hager, W.H., 1992. Energy Dissipators and Hydraulic Jumps. Springer Science & Business Media.
Hager, W.H., Hutter, K., 1984. On pseudo-uniform flow in open channel hydraulics. Acta Mech. 53, 183–200. https://doi.org/10.1007/BF01177950.
Hager, W.H., Schwalt, M., Jimenez, O., Chaudhry, M.H., 1994. Supercritical flow near an abrupt wall deflection. J. Hydraul. Res. 32, 103–118. https://doi.org/10.1080/00221689409498792.
Hardee, H.C., Dunn, J.C., 1981. Convective heat transfer in magmas near the liquidus. J. Volcanol. Geotherm. Res. 10, 195–207. https://doi.org/10.1016/0377-0273(81)90062-7.
Favalli, M., Harris, A.J.L., Mazzarini, F., Hamilton, C.W., 2009. Construction dynamics of a lava channel. Bull. Volcanol. 71, 459–474. https://doi.org/10.1007/s00445-008-0238-6.
Harris, A.J.L., Allen, J.S., 2008. One-, two- and three-phase viscosity treatments for basaltic lava flows. J. Geophys. Res. Solid Earth 113, 1–15. https://doi.org/10.1029/2007JB005035.
Harris, A.J.L., Rowland, S.K., 2001. FLOWGO: a kinematic thermo-rheological model for lava flowing in a channel. Bull. Volcanol. 63, 20–44. https://doi.org/10.1007/s004450000120.
Harris, A., Mannini, S., Thivet, S., Chevrel, M.O., Gurioli, L., Villeneuve, N., Muro, A. Di, Peltier, A., 2020. How shear helps lava to flow. Geology 48. https://doi.org/10.1130/G47110.1/4880273/g47110.
Henderson, F.M., 1966. Open Channal Flow. Macmillan Publishing Company, New York, United States of America.
Herzog, W., 2016. Into the Inferno. Netflix, United Kingdom & Austria.
Heslop, S.E., Wilson, L., Pinkerton, H., Head, J.W., 1989. Dynamics of a confined lava flow on Kilauea volcano, Hawaii. Bull. Volcanol. 51, 415–432. https://doi.org/10.1007/BF01078809.
Hidaka, M., Goto, A., Umino, S., Fujita, E., 2005. VTFS project: development of the lava flow simulation code lava SIM with a model for three-dimensional convection, spreading, and solidification. Geochem. Geophys. Geosyst. 6, 1–26. https://doi.org/10.1029/2004GC000869.
Horn, B.K.P., Schunk, B.G., 1981. Determining optical flow. Proc. SPIE 0281 281, 319–331. https://doi.org/10.1117/12.965761.
Hulme, G., 1974. The interpretation of lava flow morphology. Geophys. J. Int. 39, 361–383. https://doi.org/10.1111/j.1365-246X.1974.tb05460.x.
Huppert, H.E., Sparks, R.S.J., 1985. Komatiites I: eruption and flow. J. Petrol. 26, 694–725. https://doi.org/10.1093/petrology/26.3.694.
Huppert, H.E., Sparks, R.J.S., Turner, J.S., Arndt, N.T., 1984. Emplacement and cooling of komatiite lavas. Nature 309, 19–22. https://doi.org/10.1038/309126a0.
Ippen, A.T., Harleman, D.R.F., 1956. Verification of theory for oblique standing waves. Trans. ASCE 121, 678–694.
James, M., Carr, B., D'Arcy, F., Diefenbach, A., Dietterich, H., Fornaciai, A., Lev, E., Liu, E., Pieri, D., Rodgers, M., Smets, B., Terada, A., von Aulock, F., Walter, T., Wood, K., Zorn, E., 2020. Volcanological applications of unoccupied aircraft systems (UAS): developments, strategies, and future challenges. Volcanica 3, 67–114. https://doi.org/10.30909/vol.03.01.67114.
Jarvis, R.A., 1995. On the cross-sectional geometry of thermal erosion channels formed by turbulent lava flows. J. Geophys. Res. Solid Earth 100, 127–140. https://doi.org/10.1029/95JB00027.
Kauahikaua, J., 2007. Lava flow hazard assessment, as of August 2007, for Kilauea East Rift Zone Eruptions, Hawai'i Island. US Geol. Surv. Open-File Rep. https://doi.org/10.3133/ofr2007126 2007-1264.
Kauahikaua, J., Cashman, K.V., Mattox, T.N., Heliker, C.C., Hon, K.A., Mangan, M.T., Thornber, C.R., 1998. Observations on basaltic lava streams in tubes from Kilauea Volcano, island of Hawai'i. J. Geophys. Res. Solid Earth 103, 27303–27323. https://doi.org/10.1029/97JB03576.
Kelfoun, K., Vargas, S.V., 2016. VolcFlow capabilities and potential development for the simulation of lava flows. Geol. Soc. Lond. Spec. Publ. 426, 337–343. https://doi.org/10.1144/sp426.8.
Kerr, R.C., 2001. Thermal erosion by laminar lava flows. J. Geophys. Res. Solid Earth 106, 26453–26465. https://doi.org/10.1029/2001jb000227.
Kieffer, S.W., 1985. The 1983 hydraulic jump in Crystal Rapid: implications for river-running and geomorphic evolution in the Grand Canyon. J. Geol. 93, 385–406. https://doi.org/10.1086/628962.
Kieffer, S.W., 1987. The Rapids and Waves of the Colorado River, Grand Canyon, Arizona. U.S. Geol. Surv. Open-File Rep., pp. 87–096.
Kilburn, C.R.J., 2000. Lava flows and flow fields. In: Sigurdsson, H. (Ed.), Encyclopedia of Volcanoes, pp. 291–305 San Diego.
Kolzenburg, S., Giordano, D., Thordarson, T., Höskuldsson, A., Dingwell, D.B., 2017. The rheological evolution of the 2014/2015 eruption at Holuhraun, central Iceland. Bull. Volcanol. 79. https://doi.org/10.1007/s00445-017-1128-6.
LaViolette, M., 2017. On the history, science, and technology included in the Moody diagram. J. Fluids Eng. Trans. ASME 139. https://doi.org/10.1115/1.4035116.
Lenzi, M.A., 2001. Step-pool evolution in the Rio Cordon, Northeastern Italy. Earth Surf. Processes Landforms 26, 991–1008. https://doi.org/10.1002/esp.239.
Lesher, C.E., Spera, F.J., 2015. Thermodynamic and transport properties of silicate melts and magma. The Encyclopedia of Volcanoes. Elsevier, pp. 113–141. https://doi.org/10.1021/jp037247d.
Lev, E., James, M.R., 2014. The influence of cross-sectional channel geometry on rheology and flux estimates for active lava flows. Bull. Volcanol. 76, 1–15. https://doi.org/10.1007/s00445-014-0829-3.
Lev, E., Spiegelman, M., Wysocki, R.J., Karson, J.A., 2012. Investigating lava flow rheology using video analysis and numerical flow models. J. Volcanol. Geotherm. Res. 247–248, 62–73. https://doi.org/10.1016/j.jvolgeores.2012.08.002.
Lev, E., Oppenheimer, J., Carr, B.B., Perroy, R.L., Dietterich, H.R., Diefenbach, A.K., 2018. Assessing lava flow dynamics and rheology using sUAS data. AGU Fall Meeting Abstracts.
Lipman, P.W., Banks, N.G., 1987. A'a flow dynamics, 1984 Mauna Loa eruption. U.S. Geol. Surv. Prof. Pap. 1350, 1527–1567.
Llewellin, E.W., Manga, M., 2005. Bubble suspension rheology and implications for conduit flow. J. Volcanol. Geotherm. Res. 143, 205–217. https://doi.org/10.1016/j.jvolgeores.2004.09.018.
Macdonald, R.G., Alexander, J., Bacon, J.C., Cooker, M.J., 2013. Variations in the architecture of hydraulic-jump bar complexes on non-eroding beds. Sedimentology 60, 1291–1312. https://doi.org/10.1111/sed.12035.
Macías, J.L., Espíndola, J.M., Bursik, M., Sheridan, M.F., 1998. Development of lithic-breccias in the 1982 pyroclastic flow deposits of El Chichón Volcano, Mexico. J. Volcanol. Geotherm. Res. 83, 173–196. https://doi.org/10.1016/S0377-0273(98)00027-4.
Mader, H.M., Llewellin, E.W., Mueller, S.P., 2013. The rheology of two-phase magmas: a review and analysis. J. Volcanol. Geotherm. Res. 257, 135–158. https://doi.org/10.1016/j.jvolgeores.2013.02.014.
Magirl, C.S., Gartner, J.W., Smart, G.M., Webb, R.H., 2009. Water velocity and the nature of critical flow in large rapids on the Colorado River, Utah. Water Resour. Res. 45, 1–17. https://doi.org/10.1029/2009WR007731.
Malzman, L., 1985. Rivers of Fire (United States).
Montes, J.S., Chanson, H., 1998. Characteristics of undular hydraulic jumps: experiments and analysis. J. Hydraul. Eng. 124, 192–205. https://doi.org/10.1061/(ASCE)0733-9429(1998)124:2(192).
Moore, H.J., 1987. Preliminary estimates of the rheological properties of 1984 Mauna Loa lava. U.S. Geol. Surv. Prof. Pap. 1350-99 1569–1588.
Morrison, A., Whittington, A., Smets, B., Kervyn, M., Sehlke, A., 2020. The rheology of crystallizing basaltic lavas from Nyiragongo and Nyamuragira volcanoes, D.R.C. Volcanica 3, 1–28. https://doi.org/10.30909/vol.03.01.0128.
Neal, C.A., Brantley, S.R., Antolik, L., Babb, J.L., Burgess, M., Calles, K., Cappos, M., Chang, J.C., Conway, S., Desmither, L., Dotray, P., Elias, T., Fukunaga, P., Fuke, S., Johanson, I.A., Kamibayashi, K., Kauahikaua, J., Lee, R.L., Pekalib, S., Miklius, A., Million, W., Moniz, C.J., Nadeau, P.A., Okubo, P., Parcheta, C., Patrick, M.R., Shiro, B., Swanson, D.A., Tollett, W., Trusdell, F., Younger, E.F., Zoeller, M.H., Montgommery-Brown, E.K., Anderson, K.R., Poland, M.P., Ball, J.L., Bard, J., Coombs, M., Dietterich, H.R., Kern, C., Thelen, W.A., Cervelli, P.F., Orr, T., Houghton, B.F., Gansecki, C., Hazlett, R., Lundgren, P., Diefenbach, A.K., Lerner, A.H., Waite, G., Kelly, P., Clor, L., Werner, C., Mulliken, K., Fisher, G., Damby, D., 2019. The 2018 rift eruption and summit collapse of Kilauea Volcano. Science 363, 367–374. https://doi.org/10.1126/science.aav7046.
Ogden, C.L., Fryar, C.D., Carroll, M.D., Flegal, K.M., 2004. Mean body weight, height, and body mass index, United States 1960–2002. Adv. Data Vital Health Stat. 347, 1–17.
Ohtsu, I., Yasuda, Y., Gotoh, H., 2003. Flow conditions of undular hydraulic jumps in horizontal rectangular channels. J. Hydraul. Eng. 129, 948–955. https://doi.org/10.1061/(ASCE)0733-9429(2003)129:12(948).
Osmond, D.I., Griffiths, R.W., 2001. The static shape of yield stregth fluids slowly emplaced on slopes. J. Geophys. Res. Solid Earth 106, 16241–16250. https://doi.org/10.1029/2001JB000405.
Patrick, M., Dietterich, H., J, L., Diefenbach, A., Parcheta, C., Anderson, K., Namiki, A., Sumita, I., Kauahikaua, J., 2019. Cyclic lava effusion during the 2018 eruption of Kilauea Volcano. Science 366, 1213–1223. https://doi.org/10.1126/science.aay9070.

Pinkerton, H., Norton, G., 1995. Rheological properties of basaltic lavas at sub-liquidus temperatures: laboratory and field measurements on lavas from Mount Etna. J. Volcanol. Geotherm. Res. 68, 307–323. https://doi.org/10.1016/0377-0273(95)00018-7.

Pinkerton, H., Stevenson, R.J., 1992. Methods of determining the rheological properties of magmas at sub-liquidus temperatures. J. Volcanol. Geotherm. Res. 53, 47–66. https://doi.org/10.1016/0377-0273(92)90073-M.

Pinkerton, H., Wilson, L., 1994. Factors controlling the lengths of channel-fed lava flows. Bull. Volcanol. 56, 108–120.

Piombo, A., Dragoni, M., 2009. Evaluation of flow rate for a one-dimensional lava flow with power-law rheology. Geophys. Res. Lett. 36, 1–6. https://doi.org/10.1029/2009GL041024.

Richter, D.H., Eaton, J.P., Murata, K.J., Ault, W.U., Krivoy, H.L., 1970. Chronological narrative of the 1959–60 eruption of Kilauea Volcano, Hawaii. U.S. Geol. Surv. Prof. Pap. 537. https://doi.org/10.3133/pp537E.

Robert, B., Harris, A., Gurioli, L., Médard, E., Sehlke, A., Whittington, A., 2014. Textural and rheological evolution of basalt flowing down a lava channel. Bull. Volcanol. 76, 1–21. https://doi.org/10.1007/s00445-014-0824-8.

Roobol, M.J., Smith, A.L., Wright, J.V., 1987. Lithic breccias in pyroclastic flow deposits on St. Kitts, West Indies. Bull. Volcanol. 49, 694–707. https://doi.org/10.1007/BF01080360.

Rowland, S.K., Walker, G.P.L., 1990. Pahoehoe and aa in Hawaii: volumetric flow rate controls the lava structure. Bull. Volcanol. 52, 615–628. https://doi.org/10.1007/BF00301212.

Rowland, S.K., Garbeil, H., Harris, A.J.L., 2005. Lengths and hazards from channel-fed lava flows on Mauna Loa, Hawai'i, determined from thermal and downslope modeling with FLOWGO. Bull. Volcanol. 67, 634–647. https://doi.org/10.1007/s00445-004-0399-x.

Sakimoto, S.E.H., Crisp, J., Baloga, S.M., 1997. Eruption constraints on tube-fed planetary lava flows. J. Geophys. Res. Planets 102, 6597–6613. https://doi.org/10.1029/97JE00069.

Shaw, H.R., Wright, T.L., Peck, D.L., Okamura, R., 1968. The viscosity of basaltic magma: an analysis of field measurements in Makaopuhi lava lake, Hawaii. Am. J. Sci. 266, 225–264. https://doi.org/10.2475/ajs.266.4.225.

Siewert, J., Ferlito, C., 2008. Mechanical erosion by flowing lava. Contemp. Phys. 49, 43–54. https://doi.org/10.1080/00107510802077388.

Sonder, I., Zimanowski, B., Büttner, R., 2006. Non-Newtonian viscosity of basaltic magma. Geophys. Res. Lett. 33, 3–5. https://doi.org/10.1029/2005GL024240.

Spera, F.J., Borgia, A., Strimple, J., Feigenson, M., 1988. Rheology of melts and magmatic suspensions. 1. Design and calibration of concentric cylinder viscometer with application to rhyolitic magma. J. Geophys. Res. Solid Earth 93, 10,273–10,294. https://doi.org/10.1029/JB093iB09p10273.

Stanton, T.E., Pannell, J.R., 1914. Similarity of motion in relation to the surface friction of fluids. Philos. Trans. R. Soc. Ser. A, 214, 199–224.

Sun, D., Roth, S., Black, M.J., 2010. Secrets of optical flow estimation and their principles. Proceedings of the IEEE Computer Society Conference on Computer Vision and Pattern Recognition. IEEE, pp. 2432–2439. https://doi.org/10.1109/CVPR.2010.5539939.

Takahashi, T.J., Griggs, J.D., 1987. Hawaiian volcanic features: a photoglossary. US Geol. Surv. Prof. Pap. 1350, 845–902.

Tallarico, A., Dragoni, M., 1999. Viscous Newtonian laminar flow in a rectangular channel: application to Etna lava flows. Bull. Volcanol. 61, 40–47. https://doi.org/10.1007/s004450050261.

Tinkler, K.J., 1997a. Critical flow in rockbed streams with estimated values for Manning's n. Geomorphology 20, 147–164. https://doi.org/10.1016/s0169-555x(97)00011-1.

Tinkler, Keith J., 1997b. Indirect velocity measurement from standing waves in rockbed rivers. J. Hydraul. Eng. 123, 918–921. https://doi.org/10.1061/(ASCE)0733-9429(1997)123:10(918).

Truby, J.M., Mueller, S.P., Llewellin, E.W., Mader, H.M., 2015. The rheology of three-phase suspensions at low bubble capillary number. Proc. R. Soc. A Math. Phys. Eng. Sci. 471. https://doi.org/10.1098/rspa.2014.0557.

Walker, G.P.L., 1973. Lengths of lava flows. Phil. Trans. R. Soc. Lond. A. 274, 107–118. https://doi.org/10.1098/rsta.1973.0030.

Williams, D.A., Kerr, R.C., Lesher, C.M., 1998. Emplacement and erosion by Archean komatiite lava flows at Kambalda: revisited. J. Geophys. Res. Solid Earth 103, 27533–27549. https://doi.org/10.1029/97jb03538.

Wolfe, E.W., 1988. The Puu Oo Eruption of Kilauea Volcano, Hawaii: Episode 1 Through 20, January 3, 1983, Through June 8, 1984. U.S. Geol. Surv. Prof. Paper 1463.

Woodcock, D., 2003. A preliminary analysis of the dynamics of a channelled lava flow on Pico Partido volcano, Lanzarote, Canary Islands. Open Univ. Geol. Soc. J. 24, 8–12. https://ougs.org/files/ouc/archive/journal/OUGSJ_24_(1)_screen_res.pdf.

Woodcock, D., Harris, A.J.L., 2006. The dynamics of a channel-fed lava flow on Pico Partido volcano, Lanzarote. Bull. Volcanol. 69, 207–215. https://doi.org/10.1007/s00445-006-0068-3.

Yen, B.C., 1973. Open-channel flow equations revisited. J. Eng. Mech. Div. 99, 979–1009.